國 立 交 通 大 學
光 電 工 程 研 究 所
碩士論文

40GHz 非同步鎖模摻鉺光纖光固子雷射之研究

A study of 40GHz mode-locked
Erbium-doped fiber soliton lasers via
asynchronous mode-locking

研　究　生：邱 鐘 响

指 導 教 授：賴 暎 杰 老師

40GHz 非同步鎖模摻鉺光纖光固子雷射之研究

A study of 40GHz mode-locked Erbium-doped fiber soliton

lasers via asynchronous mode-locking

研 究 生：邱鐘晌　　　　　Student：Chung-Hsiang Chiu

指導教授：賴暎杰　　　　　Advisor：Yinchieh Lai

國 立 交 通 大 學　電 機 資 訊 學 院

光 電 工 程 研 究 所

碩 士 論 文

A Thesis

Submitted in Partial Fulfillment of the Requirements

for the Degree of Master in

The Department of Photonics and

The Institute of Electro-Optical Engineering

College of Electrical Engineering and Computer Science

National Chiao-Tung University

Hsinchu, Taiwan, Republic of China

中華民國九十五年七月

40 GHz 非同步鎖模摻鉺光纖光固子雷射之研究

研究生：邱鐘响　　　　　　　　　　指導教授：賴暎杰　博士

國立交通大學光電工程研究所

摘要

　　在本論文當中，我們透過實驗以及電腦模擬兩種方式對非同步鎖模摻鉺光纖光固子雷射作一番探索了解。實驗上我們嘗試使用非同步鎖模的方法成功的產生出重複率 20、30、40GHz 的光脈衝序列；脈寬分別為 628、596、849femto-seconds；超模抑制比都可以大於 40dB。理論模擬方面，也証實了非同步鎖模可以產生高重複率的短脈衝。我們也利用了電腦模擬，所得的結果和實驗的結果也有定性的吻合。另一方面，我們也探討了雷射共振腔中不同參數對於穩態脈衝脈寬及時基誤差的影響；相位調變深度、相位調變頻率、色散、疊加波鎖模對脈寬及時基誤差都有不同程度的影響。

A Study of 40 GHz mode-locked Erbium-doped fiber soliton

lasers via asynchronous mode-locking

Student: Chung-Hsiang Chiu   Advisor: Dr. Yinchieh Lai

Institute of Electro-Optical Engineering

College of Electrical Engineering and Computer Science

National Chiao-Tung University

Abstract

In this thesis, asynchronous mode-locked Erbium-doped fiber soliton lasers are explored in experiments and computer simulation. In experiments, we successfully generate 20, 30, 40 GHz pulse trains; the pulse widths are 628, 596, 849 fs respectively with SMSR >40 dB. In simulations, it's proved that asynchronous mode-locking is a viable method to generate ultra-short pulse trains at the high repetition rates and the results agree with those from experiments qualitatively. Besides, the effects of various cavity parameters on the pulse width and timing variation are also simulated.

致謝

　　回顧在交大這六年的時間裡，從不知道自己的興趣是什麼然後了解興趣在哪裡，這學習的過程受到許多人、事、物的影響以及幫助：感謝音樂所吳丁連老師的一場激發靈感的演講；很高興能夠加入光電所的行列，可以學習自己喜歡的物理、數學；還有當然就是光電所給我帶來的成長。這篇論文不光是只有我自己就可以完成的，還得需要許多人的幫忙才能更加完善。

　　想要感謝的人很多。首先，感謝賴暎杰老師給我這個寶貴的機會加入實驗室學習做研究並且耐心地的給予充滿啟發的指導。怎麼從無到有個想法然後付諸實際行動的研究過程是我人生中特別而重要的經驗，也因此對於研究本身產生了莫大的興趣。還有，老師以身作則謙沖自牧以及熱切學習的精神也讓我收穫良多。感謝 祁甡老師、 陳智弘老師、 林炫標老師能撥空擔任口試委員並且給予寶貴的建議，使得論文更加完善。

　　感謝實驗室項維巍學長在實驗上的指導，讓我在後來的實驗能夠逐漸地獨自處理問題，還有一些問題的討論也讓我對研究有更深入的了解。感謝陳智弘老師、魏嘉建學長、林俊廷學長和彭煒仁學長借用實驗器材，讓實驗得以順利進行。感謝光合訊公司廖仕揚先生能夠借用熔接儀器來熔接光纖。感謝實驗室徐桂珠學姊、業人豪同學、陳老師實驗室林擇雨同學和蔡昇祐同學在生活上的幫助以及一同創造出愉快的研究氣息。

　　最後，必須要感謝的就是費心栽培我的父母，讓我能夠專注在我的課業上，不用擔心生活上的問題。感謝你們的支持。感謝大家！

Contents

Chapter 1 Introduction

Chapter 2 Theories of mode-locked fiber lasers

Chapter 3 Experiment configuration and its results

Chapter 4 Simulation and some results

Chapter 5 Summary and future works

Reference of Figures

Reference of Tables

Chapter 1

Introduction

1.1 Brief Introduction

Mode-locked fiber lasers are ideal light sources for fiber-optic communication due to their fiber-type device compatibility, compactness, and better quality (almost transform-limited short pulses compared to those from laser diodes). Fiber-type devices have the advantages such as lower coupling loss and simplicity for manufacturing by splicing as well as significant nonlinear effects due to small core area and long interaction length. Mode-locked fiber lasers can generate short pulses at the high repetition rate by employing mode-locking mechanisms to establish the fixed relationship among the phases of the different frequency components (modes). A detailed introduction for the theory will be given in chapter 2.

Typically, there are two popular approaches to achieve mode-locking; one is through the active modulation and the other is through passive modulation. Active mode-locking can generate pulse trains at higher repetition rates when compared with passive mode-locking. On the other hand, passive mode-locking can generate shorter pulses when compared to active mode-locking. To generate shorter pulses at high repetition rate simultaneously, hybrid mode-locking can be used by employing the two approaches simultaneously.

However, there are still some problems. In active mode-locking, synchronization between the modulation frequency and the harmonic component of the cavity frequency must be perfectly maintained in order to achieve stable mode-locking. It is not easy to do in practice due to the fiber-type nature of typical fiber lasers; since the ambient temperature fluctuations will cause the length of the fiber cavity to change thermally, the cavity frequency components drifts in frequency and the synchronicity

is no longer maintained. Especially, longer cavity length causes larger variation, which is further enlarged at higher harmonics. Therefore, some cavity length/modulation frequency stabilization schemes are needed to be implemented to maintain the synchronization for long term operation.

In typical synchronous mode-locked fiber lasers, the required optical detection speed of the stabilization electronics is growing faster with a higher repetition rate and these high speed electronics are expensive for economic practice. Fortunately, by using asynchronous mode-locking the synchronization, in fact can be achieved more easily by detuning the modulation frequency of the phase modulator slightly off the cavity harmonic by 20~40 kHz. In this way, the 20~40kHz beating signal around DC in the electronic spectrum can be used to implement a more economic stabilization scheme with the use of only kHz electronics. It must be emphasized that asynchronous mode-locking mechanism needs intra-cavity soliton effects and guiding frequency filter effects in a complete sense, since detuning the modulation frequency in typical mode-locked fiber lasers will destroy the pulse patterns. Asynchronous mode-locked soliton fiber lasers can stably operate at a very high repetition rate and generate very short pulses in the same time with less cost.

Another merit of ASM fiber lasers is that the super mode noise in harmonic mode-locking is reduced significantly. This is because the intra-cavity pulses are solitons. The frequency shift imposed by the phase modulator will shift the noises away while the solitons can resist this frequency shift more. Finally, the noises are filtered out by the filter while the solitons can sustain. This noise clean-up effect is similar to the sliding-frequency guiding filter effect in soliton transmission systems.

In asynchronous mode-locked soliton fiber lasers, an interesting bound soliton pairs can be generated noiseless and stably. This shows that ASM soliton fiber lasers are also suitable as a reliable platform for bound states experiments, in addition to the

use as a light source in fiber-optic communication systems. Due to the diversity of the pulse properties from these mode-locked fiber lasers, there are already many reports[34,35] showing that the fiber lasers have got growing potentials in many kinds of applications, including optical metrology, ultra-fast optics, nonlinear optics, etc.

1.2 Motivation

Due to the diverse properties and growing applications of the ASM soliton fiber laser, we begin our studies by trying to understand the fundamental principles of this type of lasers. In this way, we can gain, at least, the required basic knowledge to build a real working fiber laser system at a repetition rate up to 40GHz. In the process of achieving this goal, a lot more information about the lasers can be learned and eventually more applications of the laser can be explored.
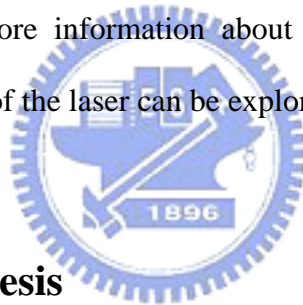
1.3 Contents of the thesis

The contents of this thesis are organized in five chapters. Chapter 1 presents a brief introduction about the development of mode-locked fiber lasers as a start. Chapter 2 is devoted to a detailed description about the theories for deeper understanding. Chapter 3 shows the experimental setup and the results based on the foregoing chapters. Chapter 4 is devoted to the simulation of the laser itself for a visualization of what is going on inside the laser cavity. Finally chapter 5 gives a summary about the future prospects of the work done here.

Chapter 2

Theories of mode locked soliton lasers

2.1 Short Pulses Generation
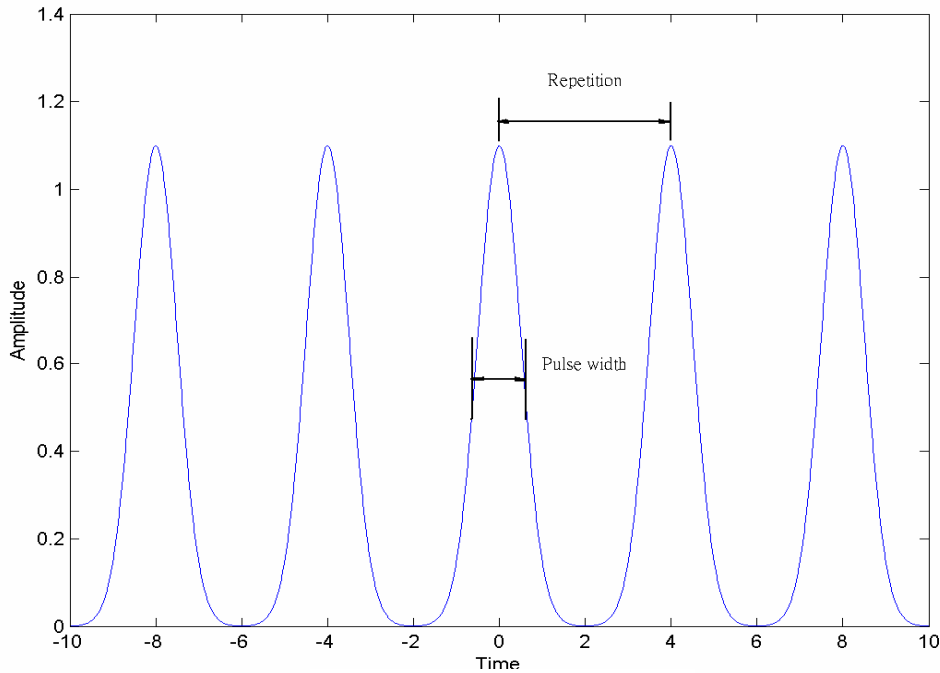
Fig. 2.1 Short pulse trains

To generate high-repetition-rate short pulses, the knowledge of what the pulses of interest explicitly look like[1] and the methods for the generation[2] of such pulses shall be needed. The mathematical function form of the pulse is in the form of Gaussian or hyperbolic secant which is a solution to the actively or passively mode-locking master equation that governs the short pulse generating laser systems. However, only when the population depletions of the gain medium and the saturable absorber are not excessive does a passively mode locked laser by slow saturable absorber have an analytical hyperbolic secant solution[2]. Many mode-locking methods have been developed and demonstrated in the literature. These will be described in the section entitled "Mode-lockers".

2.1.1 Characterization of Pulses

I. Gaussian pulses

The function form of Gaussian pulses is written[1,35] as bellows:

$$E(t) = \frac{1}{2} E_0 \exp\left[-\gamma t^2\right] \exp(j\omega_p t) \tag{2.1}$$

$$\gamma \equiv \alpha - j\beta \tag{2.2}$$

where α describes the width of the Gaussian pulse, ω_p is the carrier frequency, and β governs the frequency chirp of such pulse. The pulse width defined as the time separation between the two half-intensity points is

$$\tau_p = \sqrt{2\ln 2 / \alpha} \tag{2.3}$$

The bandwidth of such pulses can be defined as the frequency separation between the two half-power points of the optical spectra. It is known that the Fourier transform of a Gaussian function is still a Gaussian function, so the pulse spectra can be written as:

$$E(\omega) = E_0 / 2\sqrt{\pi/\gamma} \exp(-(\omega - \omega_p)^2 / 4\gamma) \tag{2.4}$$

So the bandwidth shall be

$$\Delta f_p = (1/\pi)\sqrt{2\ln 2(\alpha^2 + \beta^2)/\alpha} \tag{2.5}$$

Equation (2.3) along with (2.5) gives one of the important characteristics of a pulse, the pulse-bandwidth product. It can be written as

$$\Delta\tau_p \Delta f_p = (2\ln 2 / \pi)\sqrt{1 + (\beta/\alpha)^2} \tag{2.6}$$

Typically, for the case of Amplitude-Modulation-Active-Mode-Locking, which imposes no chirp on the pulse, $\beta = 0$, the value of the time-bandwidth product for Gaussian pulses is therefore 0.441. While for the case of Phase-Modulation-Active-Mode-Locking, which imposes a linear frequency chirp during the pulse and $|\beta| = \alpha$, assuming no dispersion and no nonlinear effects,

$$\Delta \tau_p \Delta f_p = 0.624 \, .$$

II. Hyperbolic secant function

The transform-limited sech pulse has the following function forms

$$E(t) = E_0 \sec h(t/\tau) \exp(j\omega_p t) \tag{2.7}$$

$$E(\omega) = E_0 \tau \sqrt{\frac{\pi}{2}} \sec h(\tau \pi \omega / 2) \tag{2.8}$$

$$\Delta \tau = \tau \ln \frac{\sqrt{2}+1}{\sqrt{2}-1} \cong 1.763\tau \tag{2.9}$$

$$\Delta f = \frac{1}{\tau \pi^2} \ln \frac{\sqrt{2}+1}{\sqrt{2}-1} \tag{2.10}$$

The time-bandwidth product is thus $\Delta \tau_p \Delta f_p = 0.314$.

The following figure depicts the difference between the Gaussian and hyperbolic secant pulses. It is noted that there are larger wings in sech pulses and the wings of Gaussian pulses drop abruptly due to the quadratic exponential decay.
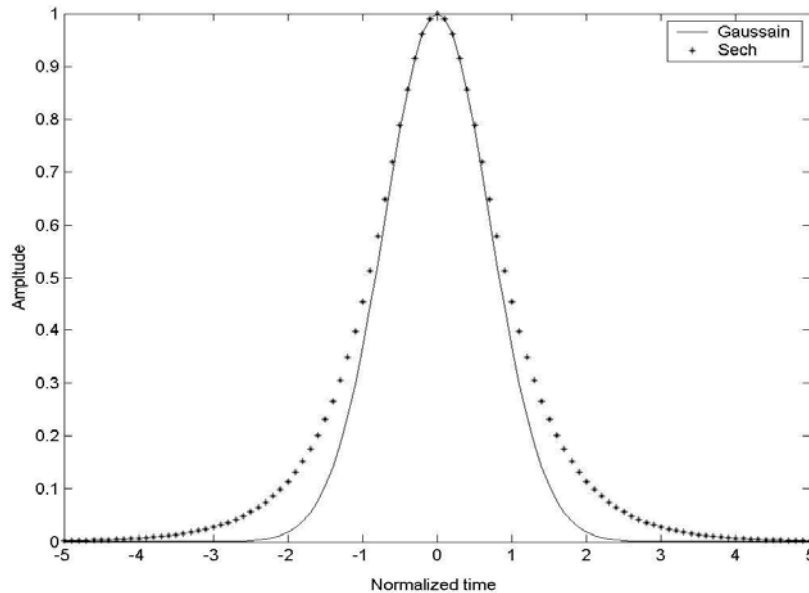
Fig. 2.1 Gaussian and sech pulse shapes

After examining the properties of the different pulses, the corresponding master equation is presented.

2.2 Master Equation

The master equation[2,3], for example, for the phase modulation case can be written as below:

$$\underbrace{T_R \frac{\partial}{\partial T} a}_{RoundTripVariation} = \left\{ \underbrace{g\left[1+\left(\frac{1}{\Omega_g}\right)^2 \frac{\partial^2}{\partial t^2}\right]}_{gain} + \underbrace{jD\frac{\partial^2}{\partial t^2}}_{Dispersion} + \underbrace{jM\cos(\Omega_m t)}_{PhaseModulator} - \underbrace{l}_{loss} - \underbrace{j\delta|a|^2}_{KerrEffect} \right\} a + \underbrace{N(T)}_{Noise}$$

where T_R is the roundtrip time; g, saturated gain; Ω_g, gain bandwidth; $D = \beta_2 L/2$, dispersion coefficient; $\delta = (2\pi/\lambda)n_2 L/A_{eff}$, Kerr coefficient; where n_2 is the nonlinear index; A_{eff} is the effective mode area; L, cavity length; M, modulation index and Ω_m, the modulation radian frequency.

It may seem very complicated at first, but with some careful inspection the master equation describes the laser cavity that contains some lumped elements: a gain medium, cavity loss, cavity dispersion effect, a mode-locker, nonlinear Kerr effect, and a spontaneous emission noise source. The total effects on the pulse formation during the roundtrip along the cavity (as shown in the right-hand-side) will be equal to the total roundtrip change (as shown in the left-hand-side). In the following sections, the action of the mode-locker is first described since it is the main mechanism for generating short pulses, we then consider the action of the other cavity elements, each of which also contributes significantly to the formation of short pulses individually or in cooperation with each other. The dispersion and nonlinear effects are omitted first for simplicity and then included afterwards.

To give an initial sense about the pulse formation, the figures in the next page depict a simple pulse formation/evolution example with respect to the round-trip time

of the cavity. The pulse grows from a very wide pulse initially and then evolves into a

shorter one afterwards.

Fig. 2.3 Pulse formation from a top view
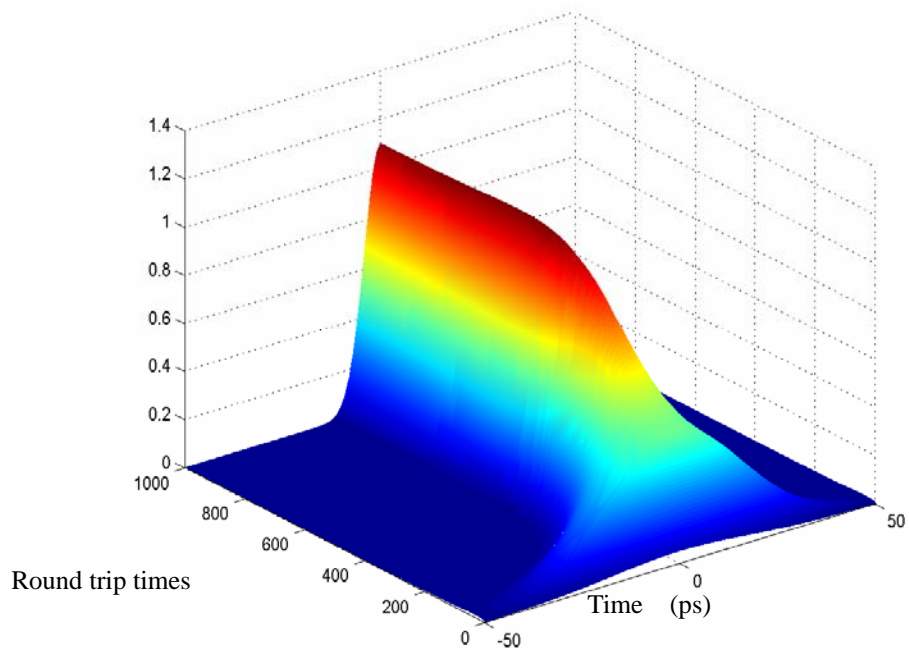
Fig. 2.4 Pulse formation from a side view

2.2.1 Mode-lockers

Assume that a laser is ready to emit CW signals at a specific wavelength. Now, if the laser has to emit pulses at a fix repetition rate, then some mechanisms are needed to be introduced into the cavity, either inside or outside the main cavity. One intuitive idea is to introduce a loss modulator in time domain inside the cavity so that the CW signal is modulated into pulses. This modulator can be either active or passive. That is, an active EO modulator driven at the desired repetition rate or a passive saturable absorber which has an intensity-dependent loss (high loss when energy is low and vice versa).
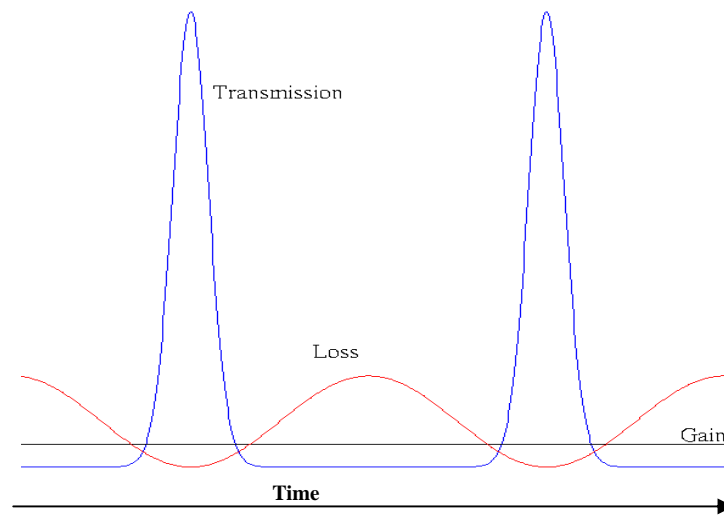
Fig. 2.5 Mode-locking principles

I. Active mode lockers
● **Amplitude modulator**

The modulation (loss) can be written as a cosinusoidal function and can be expanded to the second order of time. This approximation is valid when the pulse passes through the modulator at the maximum transmission point[1,2], which is the case in the steady case.

$$M\left[1+\cos(\Omega_m t)\right] \simeq 2 - M\frac{1}{2}(\Omega_m t)^2 \qquad (2.11)$$

The master equation can then be modified by replacing the phase modulator term with

this expression. The dispersion and Kerr effects are also omitted for the present discussion.
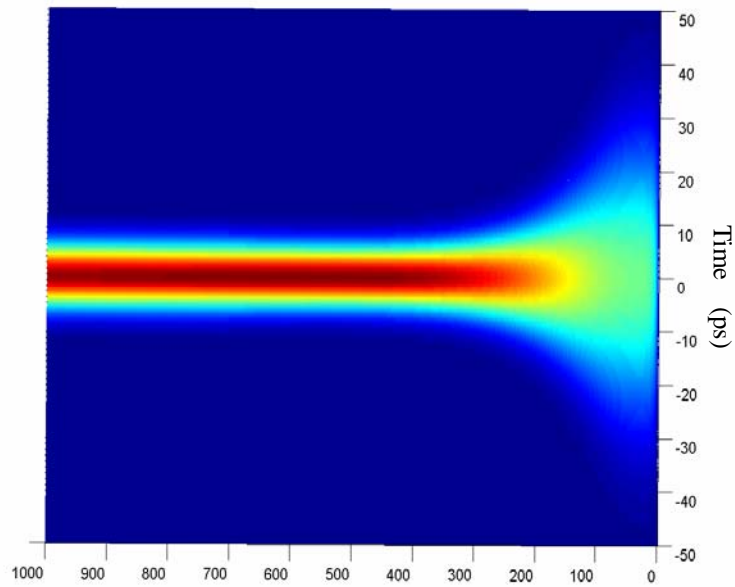
$$T_R \frac{\partial}{\partial T} a \underbrace{}_{RoundTripVariation} = \left\{ \underbrace{g\left[1+\left(\frac{1}{\Omega_g}\right)^2 \frac{\partial^2}{\partial t^2}\right]}_{gain} - \underbrace{\frac{1}{2}M\Omega_m^2 t^2}_{AmplitudeModulation} - \underbrace{l}_{loss} \right\} a \qquad (2.12)$$

The steady solution is a Gaussian pulse with a full width at 1/e intensity given by

$$\tau^4 = \frac{32g}{M(\Omega_m \Omega_g)^2} \qquad (2.13)$$

which is consistent with the Kuizenga-Siegman formula for AM mode-locking. The pulse width at FWHM differs only by a factor $\sqrt{\ln 2}$ and is given by:

$$\tau_{FWHM} = \frac{\sqrt{2\ln 2}}{\pi}\left(\frac{g}{M}\right)^{1/4}\left(\frac{1}{f_m \Delta f_g}\right)^{1/2} \qquad (2.14)$$

Typically, the pulse-width is limited by the strength of the modulator and is about picoseconds in fiber lasers. When the pulse is getting shorter, the strength of the pulse shaping effect by the modulator becomes less effective. One of the methods that can generate sub-picoseconds pulses is through passive mode-locking which utilizes self-amplitude modulation effects.
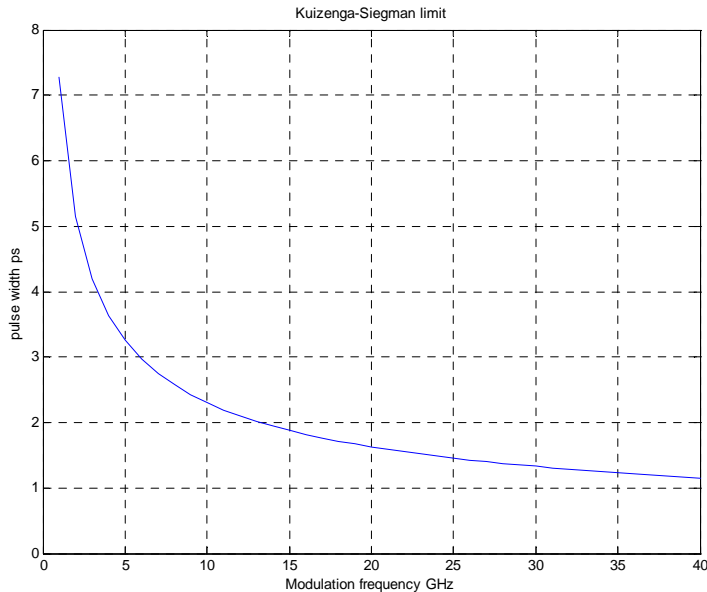
Fig. 2.6 Typical pulse width achievable in active mode-locking

The exact modulation frequency can be obtained through an analytical approach[1]

$$f_m = 1 / \left(\frac{2L}{c} + \frac{2g}{\Delta \omega} \right) \cong \frac{c}{2L} \equiv 1/T_R \qquad (2.15)$$

where

$$g = \frac{1}{2} \left(\ln \frac{1}{R} - \ln \left[1 - 8 \ln 2 M \left(f_m / \Delta f_g \right)^2 \right] \right) \cong \frac{1}{2} \ln \frac{1}{R} \qquad (2.16)$$

R is the effective reflection of a mirror including all losses. The second term in the denominator is due to the dispersion effect or linear delay imposed by the Lorentzian line of the gain which is much smaller than the cavity roundtrip time. Usually $f_m \ll \Delta f_g$, so the final approximation is valid. For Erbium fiber amplifiers, the gain bandwidth is about the order of 40nm. It is also noted from equation (2.16) that when a laser is mode-locked, the gain is pinned at the loss level. This is because the pulses carrying increasing energy will grow until the gain is saturated at the steady state.

If the modulation frequency is set to one of the harmonics of the cavity frequency (the inverse of the round trip time), $\Omega_m = N \frac{2\pi}{T_R}$, where N= 1, 2, 3,…, then the repetition rate of the laser output can be raised to a higher one and the laser is said to be mode-locked harmonically. However, there will be N unlocked groups of locked modes (i.e. super-modes) competing the gain, which will give rise to amplitude fluctuations (super-mode noises). On the other hand, the long relaxation time(1ms) of erbium fiber amplifiers makes the gain can not get recovered within one round trip time, which may lead to some pulse-to-pulse amplitude fluctuations. These problems can be solved to some extend by introducing a Fabry-Perot filter in the cavity[7] or by the incorporation of the combined SPM and spectral filtering effects[8].

The physical meaning of "mode-locker" can be appreciated in a different view when switched to the frequency domain. The "mode" represents one of cavity

longitudinal modes with different frequencies. When all of the components are superimposed together with fixed phase relationship, constructive interference somewhere and destructive interference elsewhere leads to periodical pulse formation. In this way, steady pulses at a certain repetition rate are generated.
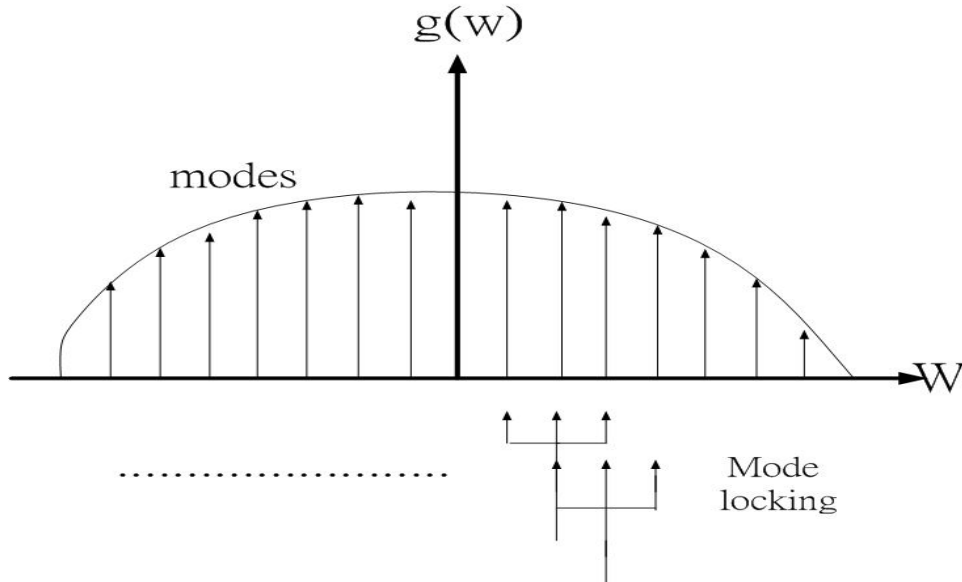
Fig. 2.7   Mode-locking illustrated in frequency domain

● **Phase modulation**

Assuming a pulse is to pass through a phase modulator, then the modified pulse can be represented as follows[1,2]

$$a' = e^{jM\cos(\Omega_m t)}a; M = \pi \frac{V_m}{V_\pi}$$

$$\Delta a = a' - a = a\left(e^{jM\cos(\Omega_m t)} - 1\right) \cong jM\cos(\Omega_m t)a$$

(2.17)

So the master equation can be written as

$$\underbrace{T_R \frac{\partial}{\partial T}a}_{RoundTripVariation} = \left\{\underbrace{g\left[1+\left(\frac{1}{\Omega_g}\right)^2 \frac{\partial^2}{\partial t^2}\right]}_{gain} + \underbrace{jM\cos(\Omega_m t)}_{PhaseModulator} - \underbrace{l}_{loss}\right\}a$$

(2.18)

The pulse-width of a Gaussian pulse solution to this equation with the phase modulator term expanded to second order is given by:

$$\tau_{FWHM} = \frac{\sqrt{2\ln 2}}{\pi}\left(\frac{g}{M}\right)^{1/4}\left(\frac{1}{f_m \Delta f_g}\right)^{1/2} \tag{2.19}$$

where the modulation frequency is

$$f_m = 1/\left[2L/c + \left(\frac{M\lambda}{\pi c}\right) + 2g/\Delta\omega\right] \cong c/2L = T_R \tag{2.20}$$

The second term of the denominator is due to the equivalent motion of the mirror. The phase modulator behaves like a vibrating mirror, which effect is small compared to the first term. The other terms are identical to the case of amplitude modulation, and the gain is

$$g = \frac{1}{2}\ln\frac{1}{R} - \frac{1}{4}\ln\left[1 - 8\ln 2M\left(f_m/\Delta f_g\right)^2 + \frac{1}{2}\left(8\ln 2M\left(f_m/\Delta f_g\right)^2\right)^2\right]$$
$$\cong \frac{1}{2}\ln\frac{1}{R} \tag{2.21}$$

The second equality is also because of the fact that $f_m \ll \Delta f_g$. Gain is pinned at the loss level of the cavity at the steady state.

Phase modulators also impose a frequency chirp over the pulse. This can be understood by expanding the phase modulation effect to the second order.

$$jM\cos(\Omega_m t) = jM\left(1 - \sin(\theta)\Omega_m t - \frac{1}{2}\cos(\theta)(\Omega_m t)^2 + \cdots\right) \tag{2.22}$$

where θ corresponds to the phase delay between the pulse and the modulation. As $\theta = 0$, it is the case at the steady state. It is the last term that gives a frequency chirp over the pulse. The first term is a phase shift and the second one is a frequency shift which vanishes when $\theta = 0$.

II. Passive mode lockers: Saturable absorbers

There are two categories of saturable absorbers, fast and slow absorbers. The main difference lies in the relaxation time relative to the pulse width. The relaxation time of the fast saturable absorber is short compared to the pulse width, while that of the slow absorber is long compared to the pulse width.

● Fast saturable absorber

The loss modulation can be written as[2,5]

$$s(t) = \frac{s_0}{1 + I(t)/I_{sat}} \tag{2.23}$$

where $s_0 (<1)$ is the linear (unsaturated) loss, $I(t)$ is the intensity, and I_{sat} is the saturation energy of the absorber. If the saturation is relatively weak, then the result can be further expended as

$$s(t) = s_0 \left(1 - I(t)/I_{sat} \right) \tag{2.24}$$

The mode amplitude is normalized so that $|a(t)|^2 = I A_{eff}$.

The transmission of the absorber becomes

$$s(t) = s_0 \left(1 - \frac{|a(t)|^2}{I_{sat} A_{eff}} \right) = s_0 - \frac{s_0}{I_{sat} A_{eff}} |a(t)|^2 \equiv s_0 - \gamma |a(t)|^2 \tag{2.25}$$

It can be seen that the loss modulation is self-intensity dependent with γ as the self amplitude modulation coefficient (SAM).

With the mode-locker term being replaced with the nonlinear term and with the first linear term s_0 being incorporated into the loss coefficient, the master equation for fast saturable absorber mode locking becomes[10]

$$\underbrace{T_R \frac{\partial}{\partial T} a}_{RoundTripVariation} = \left\{ \underbrace{g \left[1 + \left(\frac{1}{\Omega_g} \right)^2 \frac{\partial^2}{\partial t^2} \right]}_{gain} + \underbrace{(\gamma - j\delta)|a(t)|^2}_{SAM} - \left(\underbrace{l}_{loss} + j(\psi + x) \right) + jD \frac{\partial^2}{\partial t^2} \right\} a$$

$$\tag{2.26}$$

where the dispersion, nonlinearity, and phase shifts per pass are included for completeness; $\psi = (\Delta\omega_0 / c) L_{eff}$ denotes the phase shift induced by a carrier frequency shift, $\Delta\omega_0$, off from one of the Fabry-Perot resonances of the linear resonator and x denotes the phase shift during propagation.

14

The exact solution as recognized by Martinez *et al* can be written as

$$a = A \sec h(t/\tau) \exp[j\beta \ln \sec h(t/\tau)] \tag{2.27}$$

where pulse amplitude, A, pulse width, τ, and chirp parameter, β, characterize the pulse and can be obtained through substituting this ansantz into the master equation and with some manipulation the chirp parameter can be written as

$$\beta = -\frac{3}{2}\chi \pm \left[\left(\frac{3}{2}\chi\right)^2 + 2\right]^{1/2} \tag{2.28}$$

where

$$\chi \equiv \frac{\delta D_n - \gamma}{\delta + \gamma D_n} \tag{2.29}$$

and the normalized pulse width is written as

$$\tau_n = \frac{2 - 3\beta D_n - \beta^2}{\gamma} \equiv \frac{-2D_n - 3\beta + D_n\beta^2}{\delta} \tag{2.30}$$

where

$$\tau_n = \left(W\Omega_g^2/2g\right)\tau$$
$$D_n = \left(\Omega_g^2/2g\right)D \tag{2.31}$$

The net gain is found to be

$$g - l = -(1 - \beta^2)\frac{g}{\Omega_g^2\tau^2} + \frac{2\beta D}{\tau^2} \tag{2.32}$$

From equation (2.30), it is found that the pulse width is determined by the cavity parameters in the passive mode-locking case.

● **Slow saturable absorber**

For slow saturable absorber mode-locking[2,6], the equations presented above need to be modified; The gain and SAM terms must take into account the relaxation effects. The gain and the (loss) modulation is energy dependent instead of intensity dependent.

$$g(t) = g_i \exp\left(-\int_0^t dt \, |a(t)|^2 / W_g\right)$$

$$s(t) = s_i \exp\left(-\int_0^t dt \, |a(t)|^2 / W_s\right)$$

(2.33)

where g_i and s_i are the initial gain and loss before the arrival of the pulse, W_g and W_s are the saturation energies.

For this master equation to have a hyperbolic secant solution, one approximation is needed: the exponentials can be expended to second order. This is valid when the population depletion of the gain and the saturable absorber is weak. Further more, the effects of the saturable absorber must be sufficient to open up a net gain window during the pulse for a pulse to grow and a net loss window outside the pulse for noise to be suppressed. The pulse width of a pulse from a passively mode-locked laser can be of femto-seconds since when the pulse gets shorter and shorter, the strength of pulse shaping by SAM is still effective.

The repetition rate of the passively mode locked lasers is the inverse of the round trip time, $1/T_R$, which is very low with a long cavity length and can't be raised to higher repetition rate unless the laser operates in the passive harmonic mode-locking[4].

● **Artificial Fast Saturable Absorber**

In reality, there is almost no real saturable absorber with the relaxation time much shorter than 1 pico-second. Fortunately, there are some methods that use nonlinearity in corporation with some effects to act like an artificial fast saturable absorber (AFSA). These include the Additive-Pulse Mode-locking (APM)[10], and Kerr-Lens Mode-locking(KLM). The Kerr effect, which is very fast, is used in both schemes but in different ways. Other methods to achieve AFSA are by using the

nonlinear amplifying loop mirror and semiconductor saturable absorbers.

APM utilizes the nonlinear interference effect between two versions of the pulse inside the cavity. Both pulses are phase modulated by SPM to different extend during propagation so that constructive interference occurs around the peak, which leads to low loss, while destructive interference at both tails, which leads to high loss. In this way the pulse is shortened. This mechanism is suited for fiber laser due to the small core area that leads to high intensity required for SPM.

KLM, as its name suggests, utilizes self-focusing through the nonlinear refractive index, $n = n_0 + n_2 I$; higher intensity part is much focused due to higher induced refractive index and then with an aperture, high intensity part transmits at low loss and low intensity part is attenuated at high loss. In this way, pulses are also shortened. The KLM method is more suited for lasers with free space propagation.
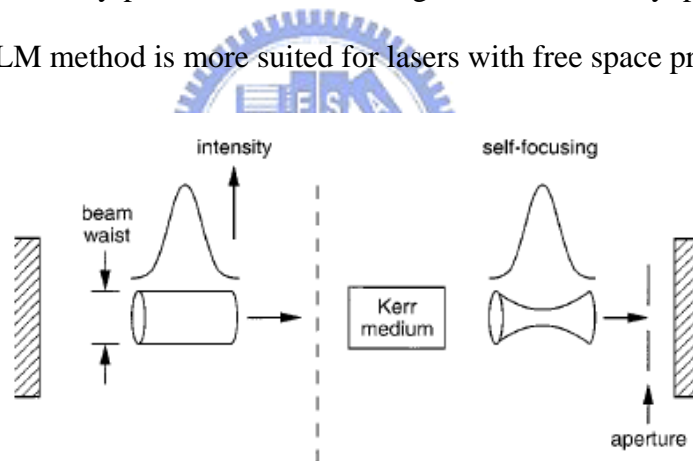
Fig. 2.8 Artificial saturable absorber realized with Kerr-lens mode-locking

There is another version of APM called "Polarization-APM", or "Nonlinear Polarization Rotation"[11].The first APM is realized with two coupled resonators in which two pulses are added together to have interference at the mirror between two resonators[12,13]. The polarization states of the two pulses have to be the same, otherwise no interference occurs. But this doesn't imply that the polarization hinders APM to take place. On the other hand, P-APM utilizes the polarization effect in a single resonator to have virtually two temporal coupled resonators by transforming a

pulse into elliptical polarization with a polarizer followed by a quarter–wave plate, thus creating a pulse in different polarization states, right-hand and left-hand circular polarization with different intensities. SPM from the isotropic Kerr medium modulates the phases unequally so that the ellipse rotates with maintained handedness and ellipticity. Then, adding two polarization components together at the polarizer where the peak of the pulse with more rotation transmits at low loss and the wings are blocked. The method is also called "Nonlinear Polarization Rotation Mode-locking".
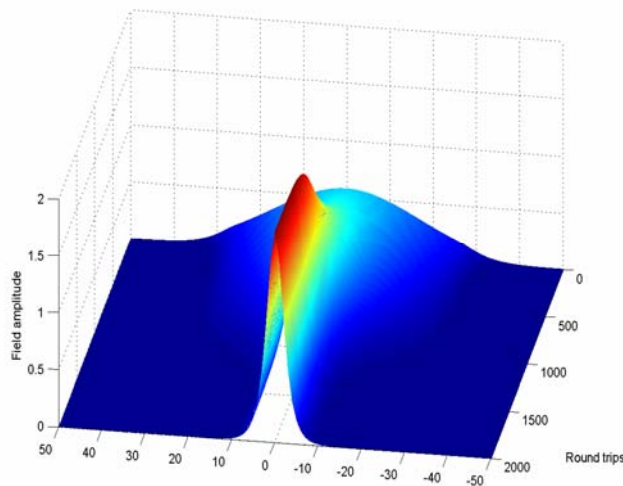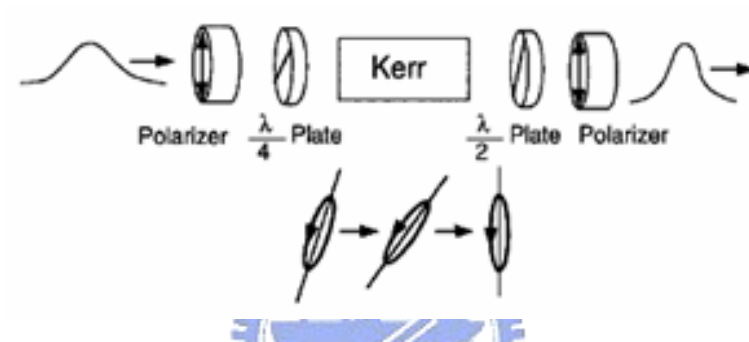
Fig. 2.9 Principles of P-APM and the pulse formation process using P-APM

2.2.2 Gain medium

In our mode locked laser system, the gain medium (Erbium-doped fiber) [14, 15] can be ideally described by a Lorentzian function

$$g(\omega) = g \left/ \left(1 + \left(\frac{\Delta\omega}{\Omega_g} \right)^2 \right) \right.$$
(2.34)

where $\Delta\omega$ denotes the frequency deviation from the central frequency of gain, Ω_g is the bandwidth of radian frequency, and g is the saturated gain which can be written as

$$g = \frac{g_0}{1 + W / E_{sat}}$$
(2.35)

where g_0 denotes the unsaturated gain, E_{sat}, the saturation energy of the gain medium. This saturation energy is dependent on the involved medium and optical frequency. It can be written as

$$E_{sat} = \frac{\hbar\omega}{\sigma} A_{eff} \frac{T_{rep}}{\tau}$$
(2.36)

where ω is the optical frequency, σ the absorption cross section, T_{rep} the time duration between pulses, A_{eff} the effective mode area and τ the life time of the populated level.

Next figure shows the process of gain relaxation of a pulsing laser for different saturation energies with all the other parameters fixed. It is noted that no matter in which cases, laser gains are pinned at loss level after more than 10 round trips. The difference is that in the case of higher saturation energy, a pulse will accumulates higher energy. So, at the fixed repetition rate, higher energy pulses will saturate the gain medium faster than lower energy pulses. The gain with a higher saturation energy is thus dropped faster than others.
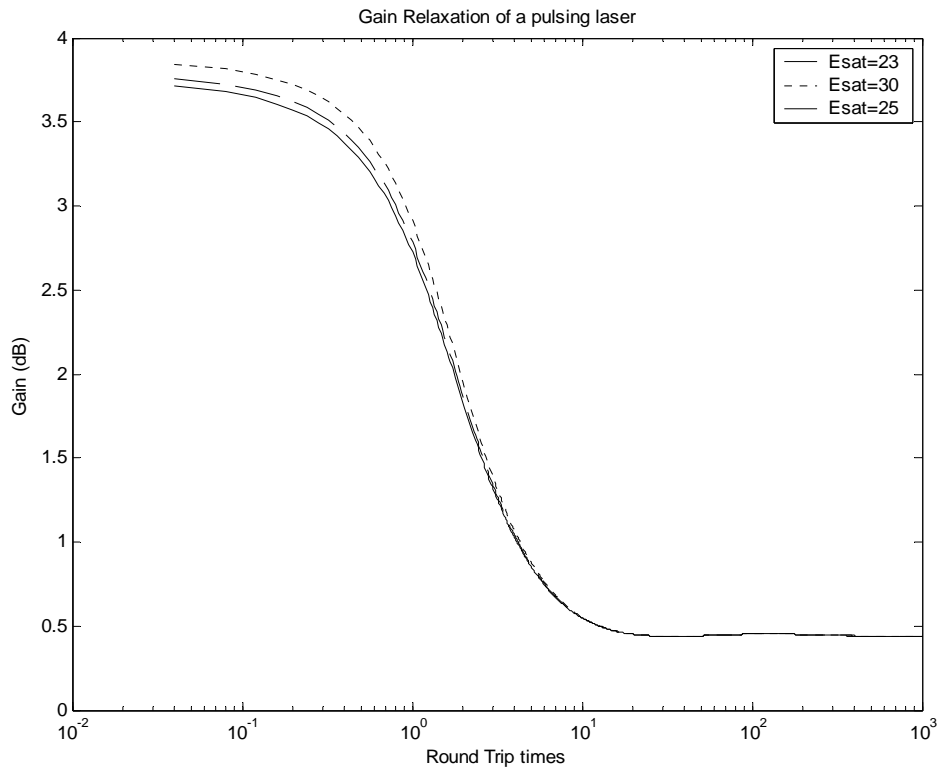
Fig. 2.10 Gain relaxation w. r. t. round trip times in different saturation energy

The pulse energy, W, inside cavity which can be written as

$$W = \int_{-T_R/2}^{T_R/2} |a(T,t)|^2 \, dt \qquad (2.37)$$

As the repetition rate is raised, the numbers of pulses inside the cavity increases by a factor of the ratio of the modulation frequency to the fundamental cavity frequency. Thus, the total pulse energy inside the cavity becomes higher if the pulse energy of a single pulse is the same.

This gain is provided by the erbium doped fiber amplifiers in our laser system. This amplifier can be modeled by the rate and propagation equations. Furthermore, this model can be approximated as a three-level system when the pumping wavelength is at 540,650,800, or 980 nm.
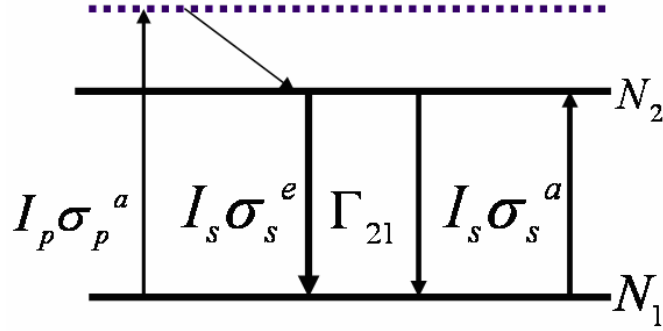
Fig. 2.11 Equivalent three level amplifiers for 980 nm pumping

In this case, from the rate equation at steady state, the population density at the population-inverted level can be written as

$$N_2(z) = \frac{\dfrac{\sigma_s^{\,a} I_s(z)}{\hbar\omega_s} + \dfrac{\sigma_p^{\,a} \sum_{u=\pm} I_{up}(z)}{\hbar\omega_p}}{\Gamma_{21} + \dfrac{\left(\sigma_s^{\,e} + \sigma_s^{\,a}\right) I_s(z)}{\hbar\omega_s} + \dfrac{\left(\sigma_p^{\,e} + \sigma_p^{\,a}\right) \sum_{u=\pm} I_{up}(z)}{\hbar\omega_p}} N \qquad (2.38)$$

and the propagation equations for the signal and the pump can be written as

$$\begin{cases} \dfrac{dI_s}{dz} = \left(N_2\left(\sigma_s^{\,e} + \sigma_s^{\,a}\right) - N\sigma_s^{\,a}\right) I_s \\[4mm] u\,\dfrac{dI_p}{dz} = \left(N_2\left(\sigma_p^{\,e} + \sigma_p^{\,a}\right) - N\sigma_p^{\,a}\right) I_p \end{cases} \qquad u = \pm \qquad (2.39)$$

where the bi-directional pumping scheme is assumed and "u" represents the pumping direction relative to the signal. Simulation can be performed on the basis of these coupled equations. From the signal propagation equation, the unsaturated gain can be written as

$$g_0 = \frac{1}{2}\int_0^L \underbrace{(N_2(z)\sigma_s^{\,e} - N_1(z)\sigma_s^{\,a})}_{population\_inversion}\Gamma_s dz \qquad (2.40)$$

where the factor of $\dfrac{1}{2}$ is due to the fact that the field is considered in the master equation instead of the intensity. It can be noted that to have gain instead of loss, population inversion is required to be achieved.

Since it is often the case that $\Delta\omega \ll \Omega_g$, this saturated gain model can be further approximated by Taylor expansion relative to the central frequency of the gain,

$$g(\omega) \cong g\left(1 - \frac{\Delta\omega^2}{\Omega_g^{\,2}}\right) \qquad (2.41)$$

As transferred to the time domain by Fourier Transform, it becomes the following form,

$$F\{g(\omega)a(T,\omega)\} \cong g\left(1 + \frac{1}{\Omega_g^{\,2}}\frac{d^2}{dt^2}\right)a(T,t) \qquad (2.42)$$

The gain is then expressed as an operator in the master equation in the time domain. The dynamic gain saturation process is neglected due to the relatively long relaxation time of most of solid state lasers. For example, the relaxation time of erbium doped fiber amplifiers is about at the order of milliseconds. In addition, this relaxation time depends on the pump power when the medium follows a three-level model.
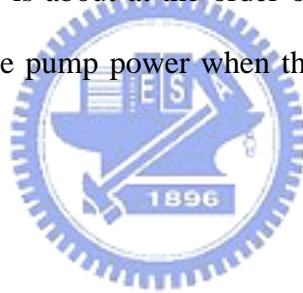
2.2.3 Dispersion and Kerr effects

So far, a simplified model for mode-locked lasers is discussed. Dispersion and Kerr effects are neglected. These effects usually exist in the cavity and thus need to be considered unless the system is dispersion free and operates under the linear regime. To consider these two effects, the master equation is added with two terms each representing these two effects respectively.

I. Dispersion

Assuming a pulse is to pass through a dispersive medium with the length L within one round trip, the changed field can be written as

$$a'(\omega) = \left[\exp(-j\beta L)\right]a(\omega) \qquad (2.43)$$

By expanding the propagation constant β to second order, we have

$$a^{'} = \exp\left(-j\frac{1}{2}\beta_2\Delta\omega^2 L\right)a \cong \left(1-j\frac{1}{2}\beta_2\Delta\omega^2 L\right)a \qquad (2.44)$$

with the constant phase term and the firs order term β_1 omitted. Inverse-Fourier transforming the equation with some manipulation, one gets

$$\Delta a(t) = a^{'} - a \cong -jD\frac{d^2}{dt^2}a(t) \qquad (2.45)$$

where

$$D = \beta_2 L / 2. \qquad (2.46)$$

II. Kerr effect

The Kerr effect manifests through the SPM effect, which can be understood by considering

$$a^{'}(t) = \exp\left(-jn\beta_0 L\right)a(t) \qquad (2.47)$$

where n is the refractive index such that $n = n_0 + n_2 I$. Omitting the constant phase term and using the normalized amplitude, $|a(t)|^2 = IA_{eff}$, we have

$$\Delta a \cong -j\delta\,|a|^2\,a(t) \qquad (2.48)$$

where $\delta = (2\pi / \lambda)n_2 L / A_{eff}$. Finally, the master equation becomes

$$T_R\frac{\partial}{\partial T}a = \left\{g\left[1+\left(\frac{1}{\Omega_g}\right)^2\frac{\partial^2}{\partial t^2}\right] - jD\frac{\partial^2}{\partial t^2} + jM\cos\left(\Omega_m t\right) - l - j\delta\,|a|^2\right\}a \qquad (2.49)$$

Since the dispersion broadens the width of the pulses, it imposes a limit on the shortest pulse achievable. However, this pulse broadening force can be reduced with a pulse narrowing force by SPM. This had been done by placing additional nonlinear mediums inside an amplitude modulated fiber laser[15] and the resulting pulse width is shorter by a factor of 2.5 than the Kuizenga–Seigman limit. The shortening effect is limited by the instabilities induced by extra SPM. Interestingly, if additional negative dispersion is introduced to balance this extra SPM, the resulting pulse is a solitary pulse with shorter width[21,22]. Under some certain conditions, solitons can be

generated.

A "solitary wave" is a propagating wave that retains its shape in the presence of dispersion and nonlinearities. A "soliton" is a propagating pulse that retains it shape in the presence of dispersion and nonlinearities even after a collision with a similar pulse. In the following sections, the formation of solitons is discussed.

III. Soliton formation

● **Area Theorem: SPM and Anomalous dispersion**

In a mathematical sense, it's known that solitons in the optical fibers are in the form of the hyperbolic secant function,

$$a(T,t) = A_0 \sec h(t/\tau)e^{-j\delta|A_0|^2 T/2T_R} \qquad (2.50)$$

which is a solution to the NLSE (Nonlinear Schrödinger Equation)

$$\frac{1}{T_R}\frac{\partial a}{\partial t} = jD\frac{\partial^2}{\partial t^2}a - j\delta|a|^2 a \qquad (2.51)$$

The solution has an important property called the "Area Theorem",

$$A_0\tau = \sqrt{-2D/\delta} \qquad (2.52)$$

After taking a careful inspection of this theorem, it indicates some important aspects of the soliton properties: the SPM has to be accompanied with anomalous dispersion to obtain a real amplitude-pulsewidth product and the required energy for soliton formation in this cavity is set by two cavity parameters.

● **Area Theorem: Energy of a soliton**

From the soliton area theorem, the energy of the fundamental soliton in the cavity is set by the net dispersion and Kerr effects of the cavity. The energy of the pulse is determined by the cavity gain and loss. If the soliton is to be generated, the cavity gain and loss together must be able to support the pulse energy set by the cavity

dispersion and Kerr effects. One of the important elements governing the gain behavior is the saturation energy. If the saturation energy of the gain medium is sufficient, then the gain medium will be able to provide the excessive gain for the required energy of fundamental soliton. At steady state, the gain is approximately saturated at the loss level and the energy of the pulse is determined, which should also be the energy of fundamental solitons of the cavity for a soliton laser. On the other hand, if the saturation energy is too low or too high, the steady state pulse may not be a soliton, either. To make a short statement, once the dispersion and Kerr parameters of the cavity are determined, the cavity gain and loss must be tailored to support solitons.

From the point of view of the balance between the SPM and dispersion, if the saturation energy is low, the gain is easily saturated and the pulse intensity doesn't initiate enough effects of SPM. Therefore, the dispersion will dominates. Otherwise, the SPM dominates.

Besides, the pulse repetition rate is also an influential effect on the gain saturation. If the repetition rate is raised higher, since the total energy inside cavity is fixed, every pulse obtains lower energy and thus the strength of nonlinearity may not be sufficient for soliton formation. The following figure shows that for a higher repetition rate the gain saturates more easily.
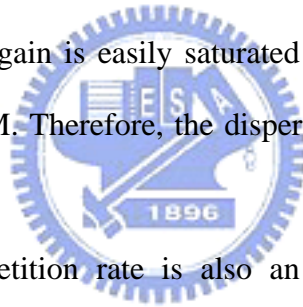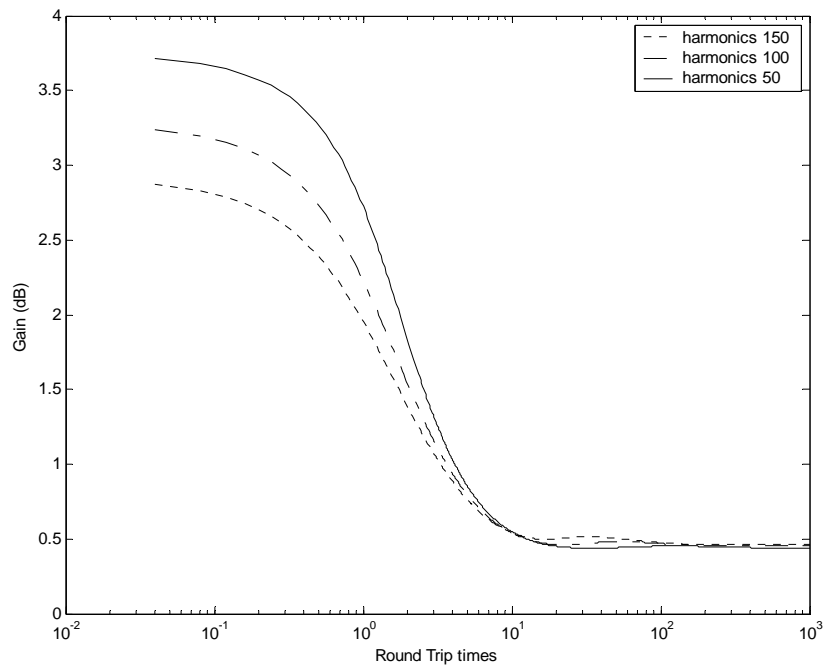
Fig. 2.12 Gain relaxation w. r. t. round trip times at different modulation frequency.

● **Perturbations**

In addition to the above implications of the area theorem, it is important to remember that the result is from the NLSE in which other actions in the cavity such as active phase modulation and SAM are not included. The NLSE in fact is an approximation of the original master equation. So, when building real fiber ring lasers, additional care must be taken to assure that the experimental settings satisfy the approximation in order to generate solitons.

● Kelly sideband

In some experiments of fiber soliton lasers, it is observed that there are some discrete sideband spectra in the optical spectrum of solitons. Some people thought that it is due to the modulation instability. But the fact is that these discrete sidebands are not located uniformly as in the case of modulation instability. It turns out that from the framework of the average soliton model[18,19,20] these non-uniform discrete sideband can be explained well[17]. Specifically, from the average soliton model it's known that the perturbations make the soliton shed continuum waves during propagation. Resonant effect occurs when one of the frequency components of the continuum waves phase-matches with that of the soliton, thus constructive interference occurs at these frequencies. The resonant frequencies in relative to the center soliton frequency can be written as follows[17,9],

$$\Delta\omega = \pm\frac{1}{\tau}\sqrt{8nZ_0/Z_a - 1}; n = 1, 2, 3, ...$$ (2.53)

where Z_0 is the soliton period defined as

$$8Z_0 = 4\pi\tau_p^2/|k''|$$ (2.54)

Z_a is the amplifier period and τ is the pulse width. Note that in the limit of $Z_0 \gg Z_a$ as in the case of broad pulses, the sidebands locate so far off the center frequency so that no sidebands occur. The following plots from Ref[17] clearly demonstrates this phenomena.
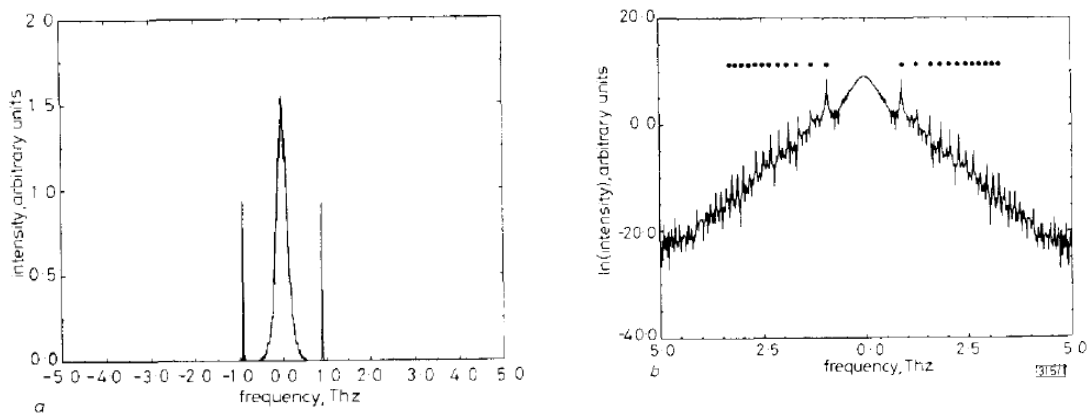

Fig. 2.13 Kelly side bands. a. Intensity plot. b. Log (intensity) plot. ' · ' indicates the position according to equation (2.53)

27

An interesting question arises when the picture is transferred to the time domain: what does the pulse look like when this resonant instability occurs? Since it is due to the phase matching between the continuum waves and solitons, we may think that there is something around the bottom of the pulse, that is, these sidebands may appear as a pedestal under the pulse and contain considerable energy.

Another question follows what is the influence of this resonant instability on soliton lasers? For a cavity with a fixed dispersion, the continuum limits the obtainable shortest pulse. And from the soliton area theorem, this implies that the peak power is lower and the average output power is decreased. It seems that having a longer soliton period through decreasing dispersion can avoid this instability. However, doing this reduce the energy of soliton due to the soliton area theorem. So, dispersion is to be optimized between these two extremes.

After going through the process of soliton formation and the related properties, it is important to keep in mind that the soliton effect has been used in mode-locked lasers to further shorten the pulse width beyond the Kuizenga–Seigman limit. Experiments[22] by D. J. Jones, H. A. Haus, and E. P. Ippen *et al* show that by using soliton-like compression the resultant pulse width is reduced by a factor of 4.4 below the Kuizenga–Seigma limit in an amplitude modulated mode-locked fiber laser. However, super mode suppression ratio is only 20~30dB from the 5GHz harmonic.

2.2.4 Asynchronous Mode locking

In a phase-modulated mode-locked soliton laser experiment [23], an interesting asynchronous modulation has been used through tuning the modulation frequency slightly off the harmonic by 5-20 kHz. This asynchronization mechanism provides pulse initialization, noise clean-up, and new form of pulse timing stabilization while not destroying the soliton pulse. The resulting pulse-width was of pico-seconds at 1GHz with the frequency spectra oscillating at 15 kHz. No long term stabilization schemes (temperature or modulation frequency) were used in that experiment.

The theory for ASM[25] indicates that soliton formation is possible in a synchronously phase-modulated mode-locked laser under the condition that the required net gain for noise to grow is greater than that for soliton to form, which will be given in equation (2.60). This theory also indicates that asynchronous mode-locking allows soliton formation with an additional requirement that the noise decay rate is faster than the detuning rate, indicated by equation (2.61) later. By applying this asynchronization scheme, our previous work[24] successfully generated 10 GHz 816 fs soliton pulse train with SMSR>70dB from a hybrid mode-locked fiber laser. In the following paragraphs, this theory is introduced.

I. Main Theory

To model this frequency detuning action into the master equation, a time delay is to be added between the pulse peak and the modulation peak. Originally, master equation is modeled by assuming that the pulses pass through the modulation peak. So merely setting the modulation frequency to a detuned one is not sufficient. Based on this observation, the master equation can be written as follows: (note that when there is no frequency detuning, the equation is the same as for synchronous mode-locking)

$$T_R \frac{\partial}{\partial T} a = \left\{ g \left[1 + \left(\frac{1}{\Omega_g} \right)^2 \frac{\partial^2}{\partial t^2} \right] + jD \frac{\partial^2}{\partial t^2} + jM \cos\left(\Omega_M \left(t + \Delta T(T) \right) \right) - l - j\delta \, |a|^2 \right\} a \quad (2.55)$$

where
$$\Delta T(T) = -\frac{\Omega_H - \Omega_M}{\Omega_M} T \quad (2.56)$$

Equation (2.56) represents the time shift imposed by the detuned modulation frequency.

In ASM, there is a timing variation, $\Delta t(T)$, resulting form the frequency shift off the nominal carrier frequency of the pulse due to the detuned modulation frequency; the carrier frequency shift results in a change in group velocity. This frequency shift, Δp, can be derived from the equation of motion for the frequency deviation of the soliton. This carrier frequency shift was observed in an experiment[23] by C. R. Doer *et al.* and can be derived from equation (2.56) by using the soliton perturbation theory[3] with the results as

$$T_R \frac{\partial \Delta t(T)}{\partial T} = 2 \, |D| \, \Delta p \quad (2.57)$$

where
$$\Delta p = -\tau_0 M \Omega_M \sin(\Delta \Omega T) \quad (2.58)$$

and
$$\tau_0 = \frac{3 \Omega_g^2 \tau_s^2}{4g} \quad (2.59)$$

τ_s is the pulse width.

Last but not least, the time delay related to the frequency shift should not be additionally added to (2.56) because (2.56) has already implicitly included this frequency shift effect. This can be understood by inspecting equation (2.22).

II. Noise cleanup effect

The ASM mechanism can provide noise cleanup effects. Since in ASM the phase modulator imposes frequency shifts on both solitons and noises and the soliton can recover after being perturbed, so after some roundtrips the noises drift out of synchronism due to GVD and then filtered out by the filter. This effect sets the lower

limit of the cavity GVD and can be written as

$$\text{Re}\left\{\sqrt{\left(\frac{g}{\Omega_g{}^2}+jD\right)\left(j\frac{M\Omega_m{}^2}{2}\right)}\right\}>\frac{2}{3}\frac{g}{\Omega_g{}^2\tau_s{}^2} \qquad (2.60)$$

This inequality is obtained from the fact that the required net gain for noises is higher than that for solitons in order for solitons formation to be possible. It seems that with higher GVD, less noise we will have. But remember that from the soliton area theorem, the required soliton energy is raised accordingly. Thus the GVD is to be optimized.

III. The limits of the detuning range

In fiber-optic soliton transmission, ASE induced noises from periodic amplifiers for compensating loss will cause the random frequency shifts of the soliton, which in turn changes the group velocity of the solitons and leads to the random timing jitter[26]. This timing jitter can be controlled, not eliminated, by using a sliding-frequency guiding filter[27,28,29]. In ASM fiber lasers, there is a similar mechanism in which a fixed-frequency filter is used and the solitons with a sliding carrier frequency, Δp, due to the detuning play the role of sliding frequency. This timing stabilization must be frequent enough so that the pulse timing is periodically refreshed. This requirement imposes the lower limit of the detuning frequency. The upper limit of the detuning is obtained from the fact that the detuning rate should be much slower than the noise decay rate for soliton formation to be possible in asynchronous mode locking, which can be quantized as

$$|\Delta\Omega_{\text{lim}}|\ll\frac{2\pi}{T_R}\text{Re}\left\{\sqrt{\left(\frac{g}{\Omega_g{}^2}+jD\right)\left(j\frac{M\Omega_m{}^2}{2}\right)}\right\} \qquad (2.61)$$

If the detuning frequency is over this limit, noise grows and the pulse train is destroyed. Note also that when the laser is operating at a higher repetition rate, the
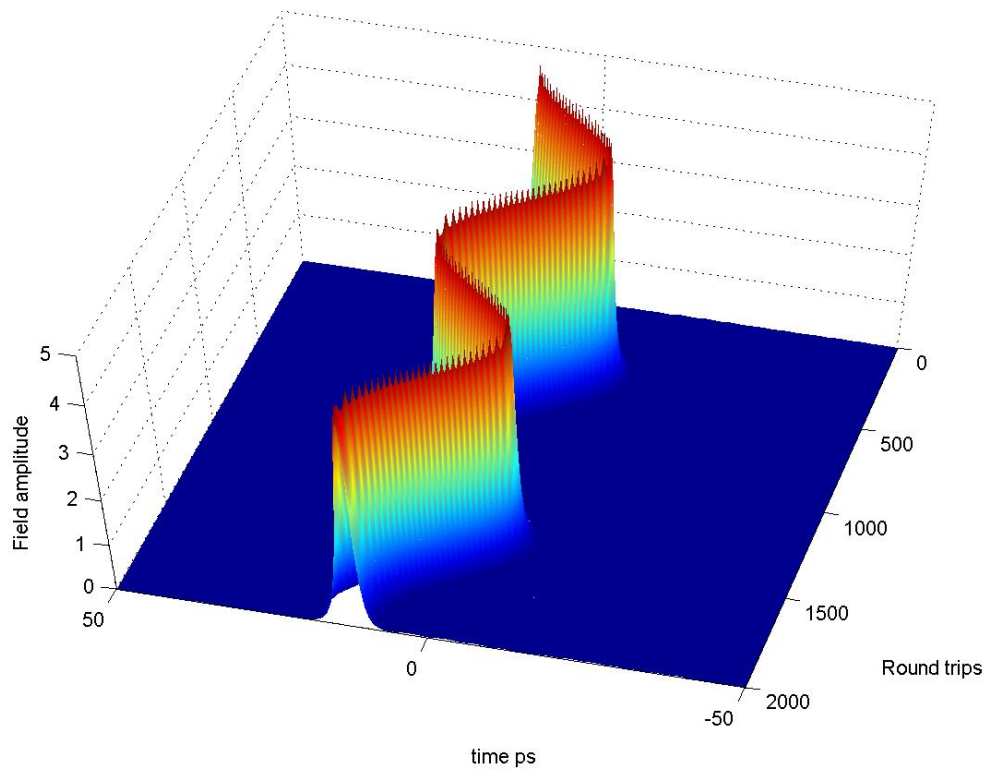
acceptable detuning range is wider.

Fig. 2.14 ASM pulse timing variation.

The figure above shows the simulation of the resultant pulse evolution by using the standard split-step FFT method. The cavity round trip time is 25 ns and the detuning frequency is 40 kHz, corresponding to a period of 1000 round-trips. The peak-to-peak timing displacement is ~20 ps. The FWHM pulse width is 1.53 ps at 1 GHz. This shows that ASM is indeed a viable method for the generation of ultra-short pulses when compared with typical synchronous mode-locking. In the next chapter, our experiment setups and results will be presented.

Chapter 3

The experiment settings and results
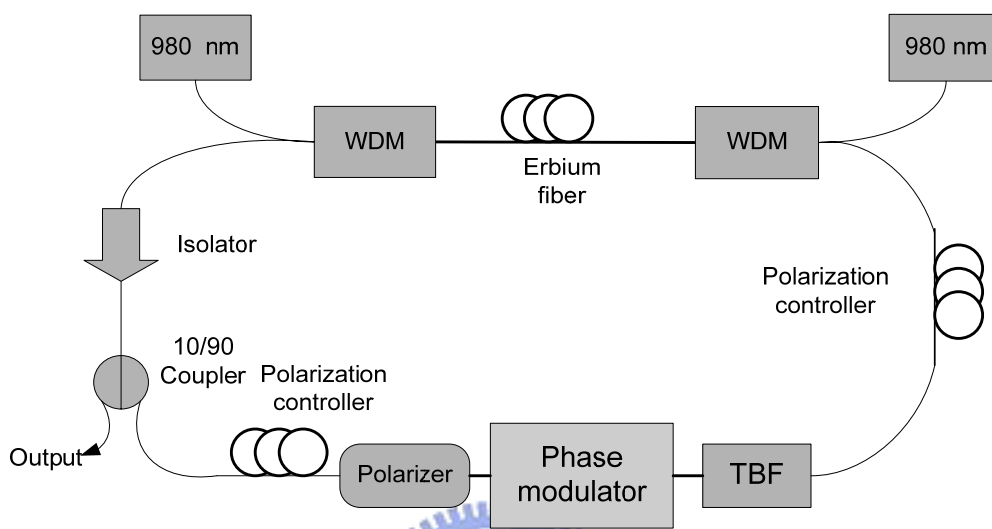
3.1 The structure of the ASM soliton lasers

Fig. 3-1. Experiment setup. TBF stands for tunable band-pass filter

The experimental setup of the ASM fiber laser is shown in the figure above. The phase modulator needs a polarizer in the input end to align the polarization axis of pulses with that of the EO crystal. The isolator is for single direction wave propagation to prevent spatial hole burning and is polarization-independent since the polarizer and the phase modulator provides enough polarization dependent loss for Polarization Additive Pulse Mode-locking (P-APM). The two polarization controllers are placed in the cavity to adjust the polarization state for achieving P-APM. A tunable band-pass filter is introduced in the cavity in cooperation with SPM to suppress super-modes in harmonic mode-locking and also provides the sliding-frequency guiding-filter effects for noise clean-up. A section of 10 meters Erbium-doped fiber pumped by two 980 laser diodes acts as the gain medium of our laser. Finally, the output coupler extracts 10% of the powers in the cavity. The total cavity length is 35.24 meters with cavity fundamental frequency 5.33 MHz. The

estimated total dispersion and Kerr coefficient are -0.023 ps^2 and 0.085 W^{-1} respectively. The values and units of parameters for some devices used in the experiments are estimated as below.

Table 3.1 Estimated values of parameters

SMF	Value	Unit
β_2	-0.02328	ps^2/m
V parameter	2.0345	
r_{core}	4.1	μm
A_{eff}	82.32	μm^2
δ	0.00122	W^{-1}/m
EDF		
β_2	0.05164	ps^2/m
δ	0.00629	W^{-1}/m
I_{sat}	70.39949	MJ/m^2s
σ_s^a	1.81367342e-25	m^2
σ_s^e	3.162998853e-25	m^2
σ_p^a	1.9e-25	m^2
σ_p^e	0	m^2
$\Gamma_{overlap}^s$	0.4	
$\Gamma_{overlap}^p$	0.64	
$\Delta\lambda_g$	30	nm
τ_{life}	10	ms
A_{eff}^s	16	μm^2
A_{eff}^p	7	μm^2
Optical band-pass filter		
$\Delta\lambda_f$	12.5	nm
loss	3	dB
Phase modulator		
insertion loss	2.8	dB
Vpi	4.7@1GHz	volts

Note:

$$D = -\frac{2\pi c}{\lambda^2}\beta_2 ; [D] = \frac{ps}{km*nm}, [\beta_2] = \frac{ps^2}{m}, [c] = m/s, [\lambda] = nm$$
$$\beta_2 = -1.2745*10^{-3} D @ 1550nm$$

3.2 The results at 20 GHz

The resultant optical bandwidth is 4 nm which corresponds to a 628-fs soliton pulse, assuming transform limited sech^2 pulses. The SMSR is greater than 40 dB with the resolution bandwidth of 300 kHz. If the resolution bandwidth is reduced, higher SMSR is observed. The average output power is 12.22 mW with 440 mW pump power. This pulse train is obtained when the detuning frequency is 30 kHz. Fig. 3.2 shows the optical spectrum and Fig. 3.3 shows the RF spectra with the frequency spans of 50 MHz and 100 kHz. The laser can operate stably for tens of minutes and needs cavity stabilization for long term operation.
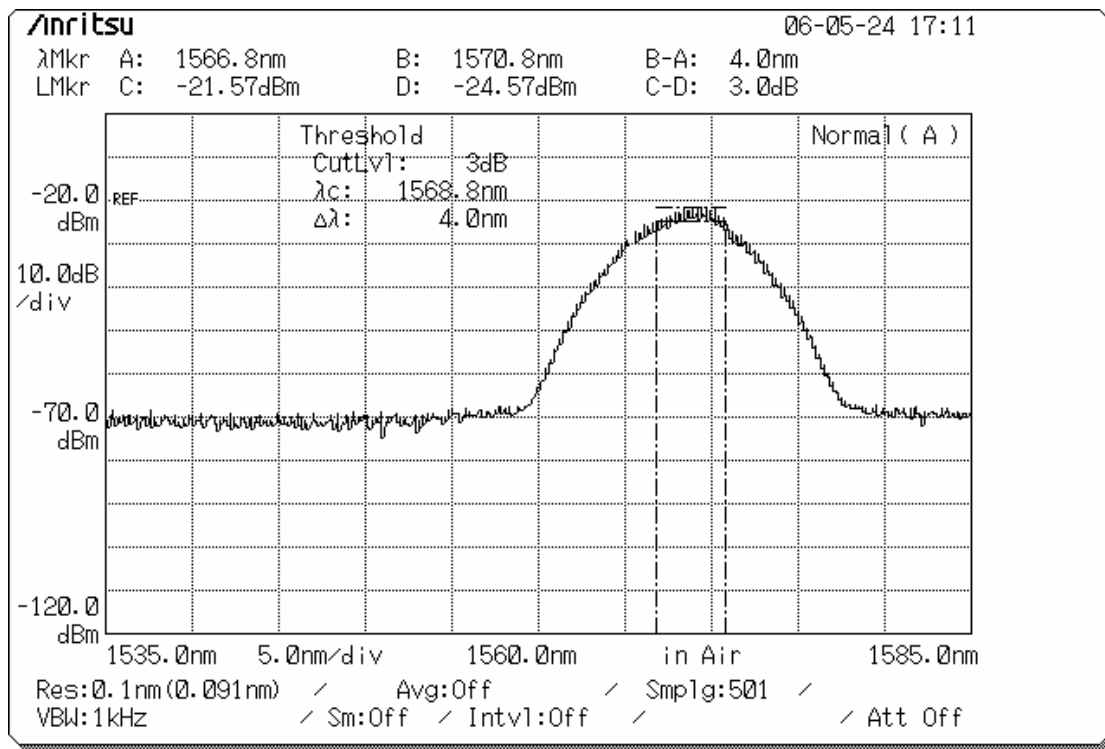

Fig.3.2   The optical spectrum. The bandwidth is 4 nm directly from the
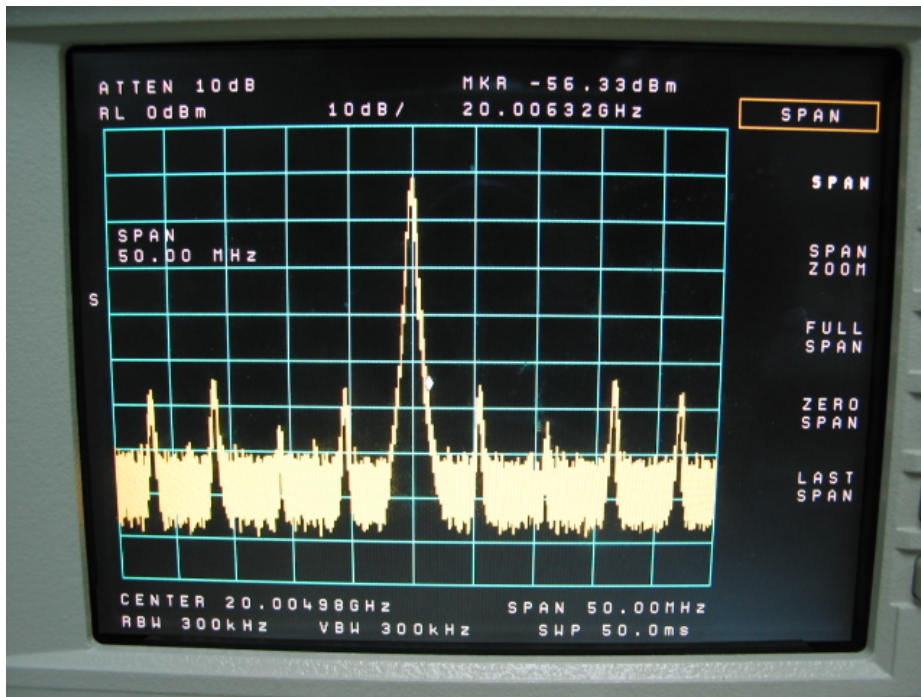
laser cavity.

Fig 3.3 The RF spectrum with span 50. SMSR >40dBMHz
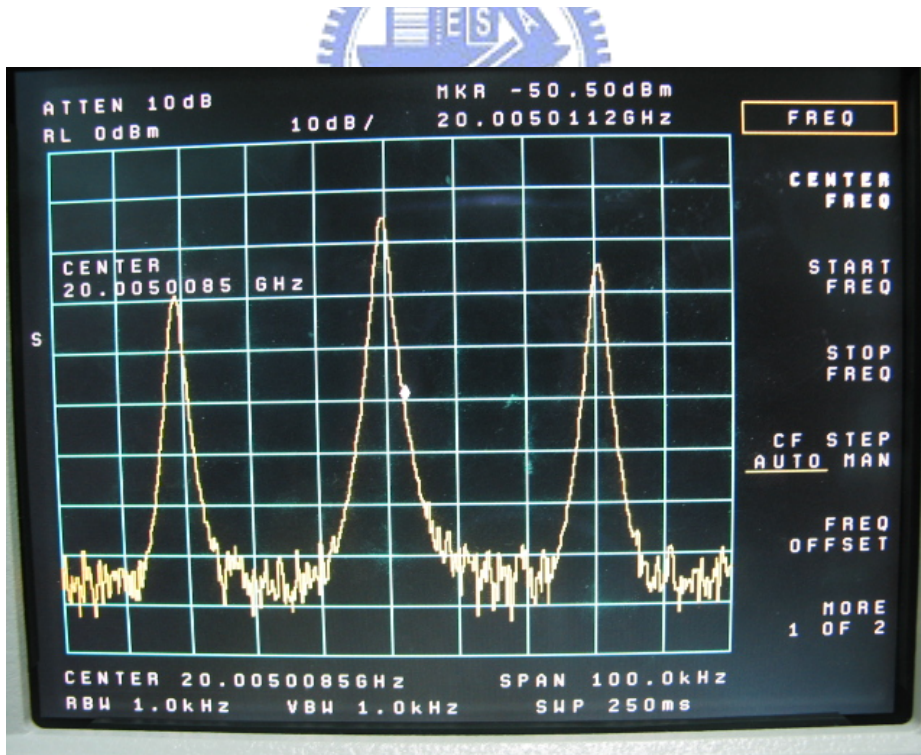
(300kHz resolution bandwidth)

Fig3.4   The RF spectrum with span 100 kHz. A 30 kHz   frequency

detuning between the cavity harmonic and the modulation

frequency is shown.

3.3 The results at 30 GHz

When the modulation frequency is detuned from the 30GHz cavity harmonic component by 20 kHz, the resulting optical bandwidth is 4.24 nm directly from the laser cavity. This corresponds to a 596 fs pulse width assuming transform-limited sech pulse. The SMSR is at least greater than 40 dB with the resolution bandwidth of 300 kHz. Fig. 3.5 shows the optical spectrum and Fig. 3.6-7 show the RF spectra with the frequency spans of 50 MHz and 100 kHz. The beating signal between the harmonic component and the modulation frequency is about 20 kHz. This is the characteristic of ASM soliton lasers. The output power from the 10% coupler is 24.37mW with 732 mW pump power.
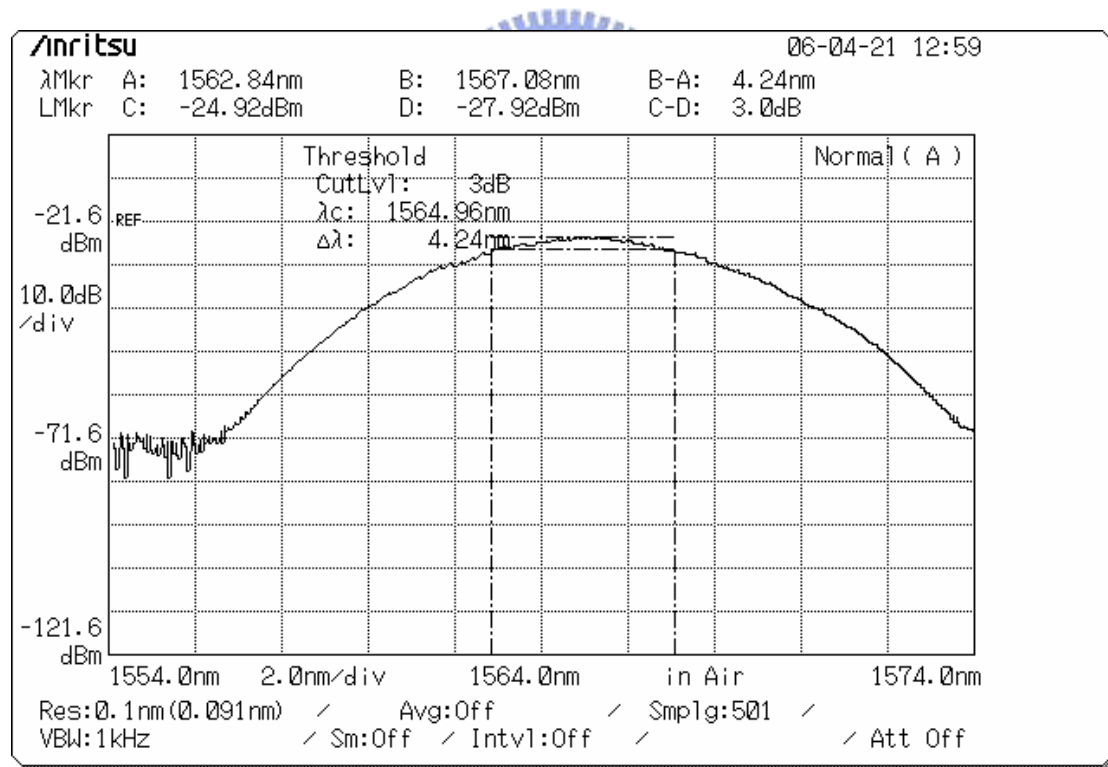

Fig. 3.5 The optical spectrum. The bandwidth is 4.24 nm directly from the laser cavity.
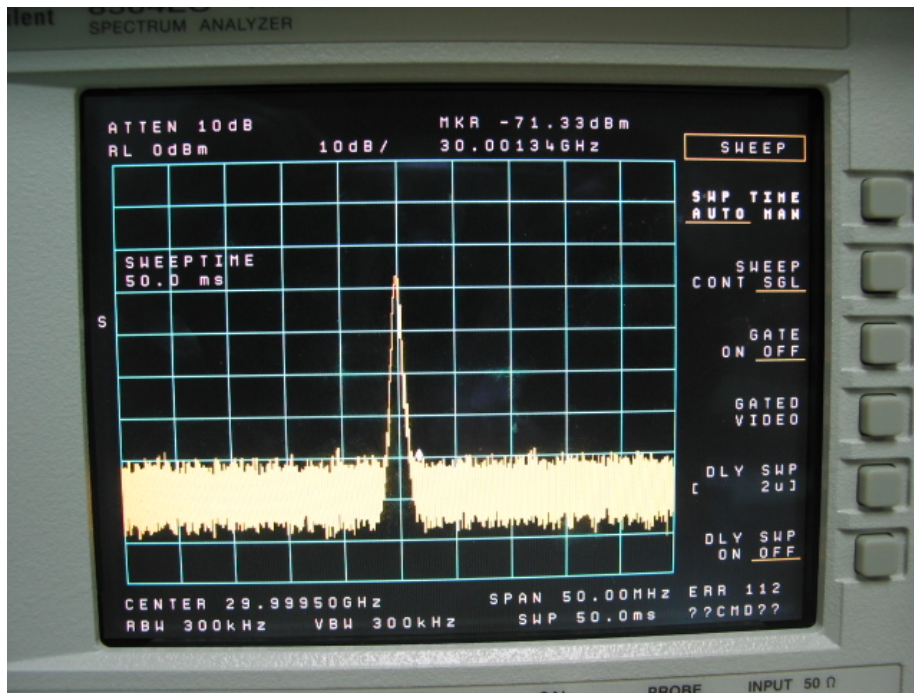
Fig.3.6 The RF spectrum with span 50. SMSR >40dBMHz
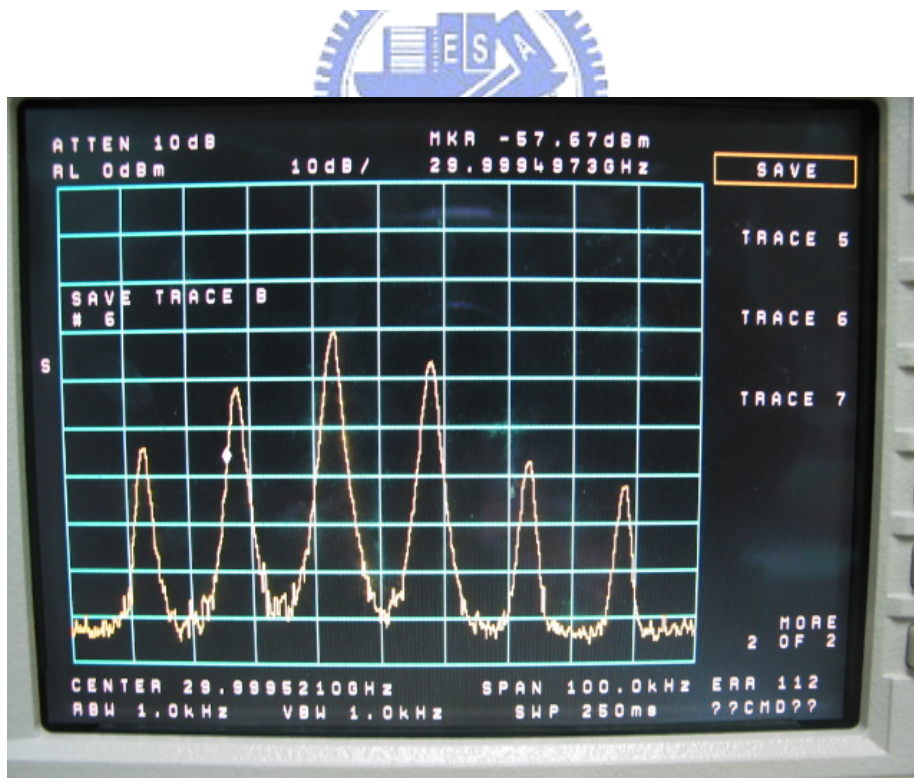
(300kHz resolution)

Fig. 3.7   The RF spectrum with span 100 kHz. A 20 kHz   frequency

detuning between the cavity harmonic and the modulation

frequency is shown.

3.4.1 The results at 40 GHz

For the available maximum pumping powers of 900 mW, the laser cavity used to generate 20 and 30 GHz pulse trains needs more pumping power than 900 mW to operate at 40GHz. Due to the fixed maximum power available inside the cavity, to generate 40 GHz pulse trains energy for each soliton needs to be reduced through either decreasing the dispersion or increasing the nonlinearity. The following figures show the resultant optical spectra and RF spectra from a cavity with less dispersion.

The pumping power is 880 mW and the output power is 25 mW. The modulation frequency is 39.999 GHz with <60 kHz detuning frequency away the harmonic frequency. The total cavity length is 32.24 meters (shorter SMF). The optical spectrum is 2.92 nm which is shorter due to lowered soliton energy. The SMSR of 40 dB is obtained.
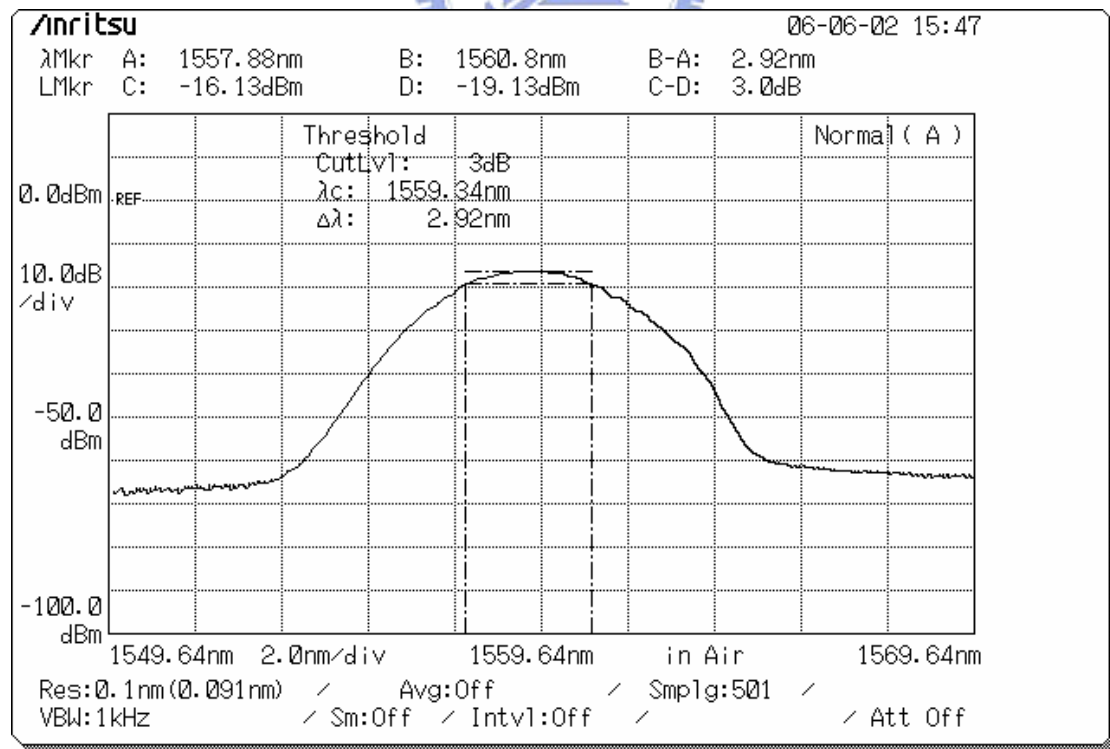

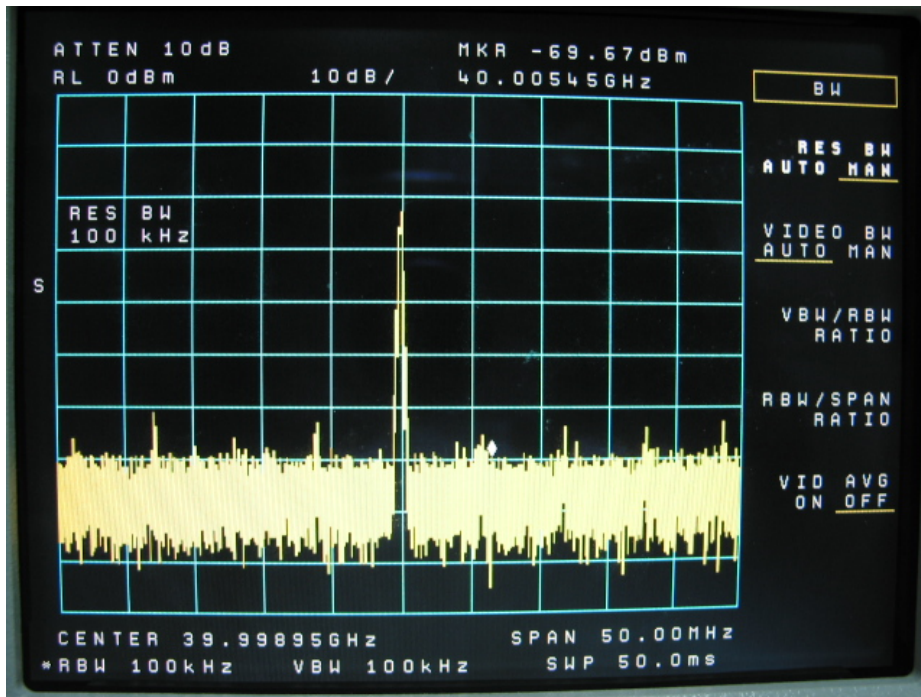Fig. 3.8 The optical spectrum. The bandwidth is 2.92 nm from the laser cavity.

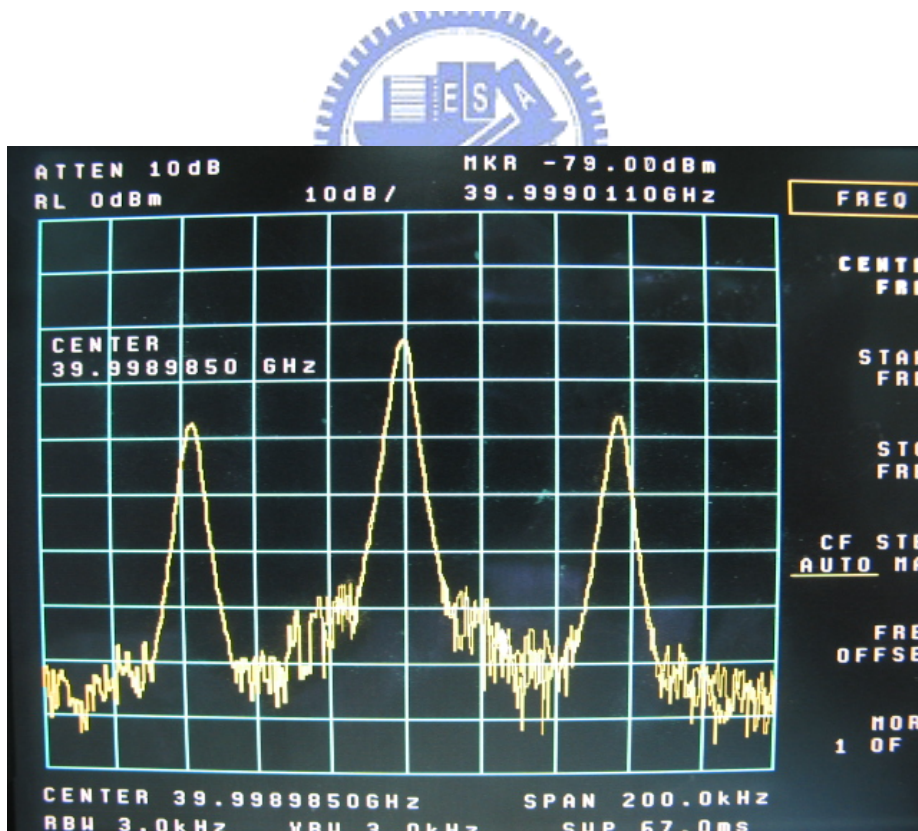Fig. 3.9 The RF spectra with the span 100 kHz.

Fig. 3.10 The RF spectra with the span 300 kHz. A 30 kHz   frequency detuning

between the cavity harmonic and the modulation frequency is shown.

3.4.2 Results from typical synchronous mode-locking

For comparison, the resulting optical spectrum by synchronous mode-locking is shown below along with the SMSR. The width at 3dB of the optical spectrum directly from the laser cavity is 2.04 nm with ~0.4 nm modulation period due to 40 GHz modulation. The SMSR is >50 dB with the resolution bandwidth of 100 kHz. The output power is 24.7 mW with the total pump power of 888 mW. The optical bandwidth from synchronous mode-locking at 40 GHz is 2.04 nm which is smaller than that from ASM. The ASM can generate shorter pulses.
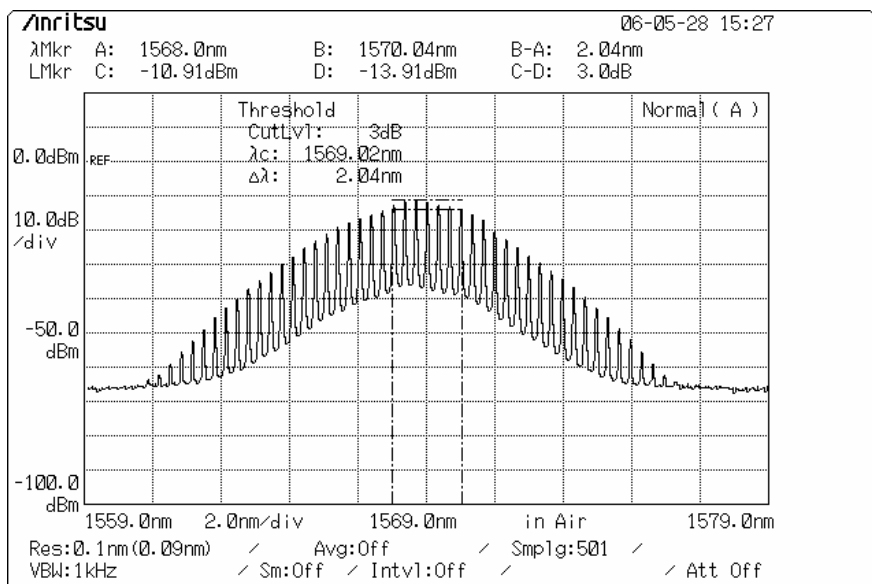

Fig. 3.11 The optical spectra. The bandwidth is 2.04 nm from the synchronously
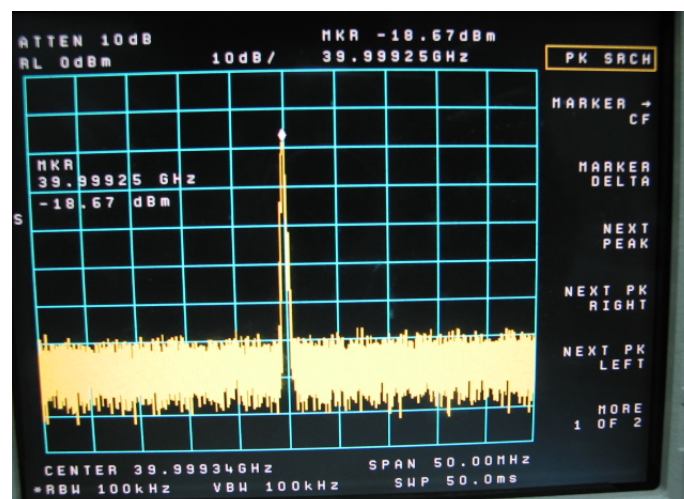mode-locked laser cavity.

Fig. 3.12 The RF spectra with 50 MHz span and 100 kHz
resolution bandwidth.

3.4.3 Bound solitons in FM synchronous mode-locking

In this FM fiber laser, bound state of pulses can be generated with good quality at a very high repetition rate. Figures below show the optical spectra and the RF spectra at 40GHz in synchronous mode-locking. From the interferential optical spectrum modulation, the corresponding pulse separation is about 2.35 ps. The SMSR is >45 dB at the resolution bandwidth of 100 kHz. The phase modulation is very important for the formation of bound state[31].
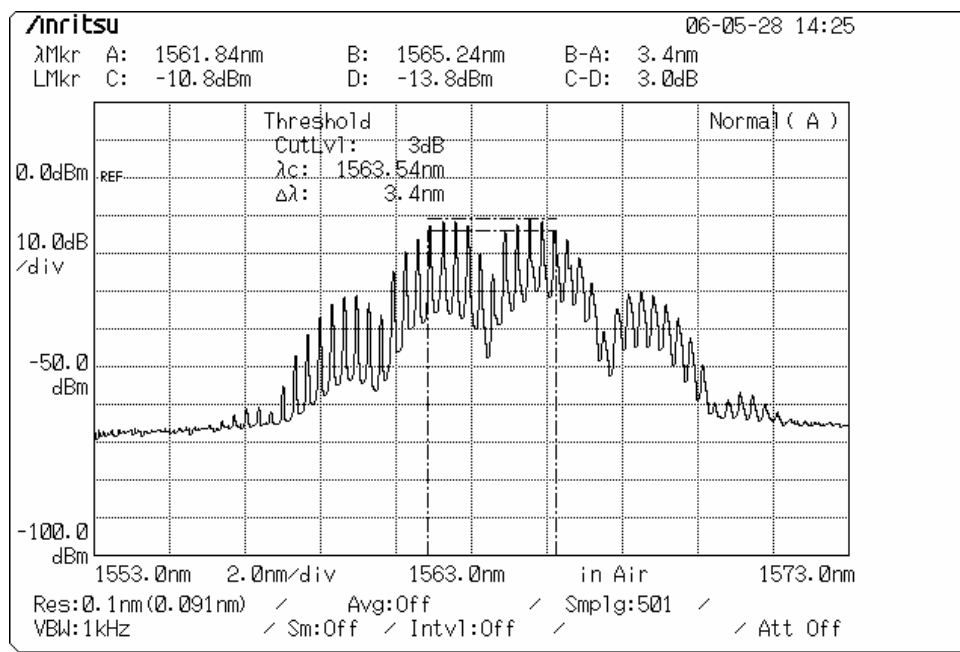

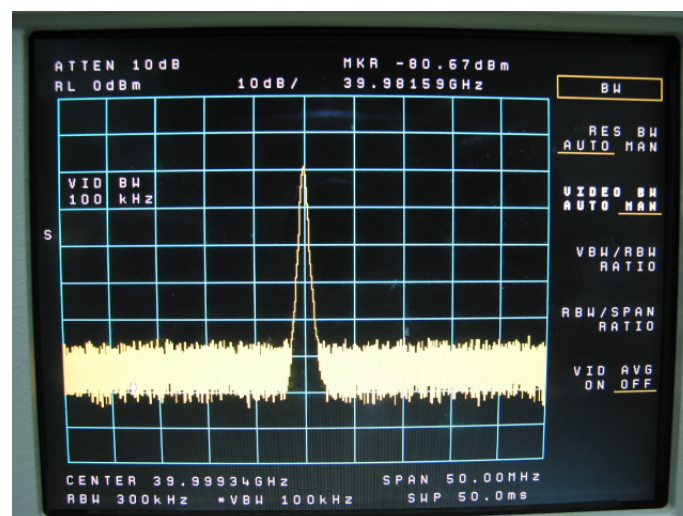Fig. 3.13 The optical spectra. The modulation period is 3.4 nm.

Fig.3.14 The RF spectra with the 50 MHz span and the 100 kHz

resolution bandwidth.

3.5 Long term stabilization

Due to the ambient temperature fluctuations of the operation condition, the cavity length fluctuates accordingly. For example, for a typical mode-locked silica-fiber laser of the length 50 m and a thermal expansion coefficient of $1.1*10^{-5}$ /^{o}C, the resulting frequency drift at the 8-GHz cavity harmonic is ~60 kHz. At higher repetition rate, this cavity harmonic frequency drift is even larger. Therefore, stabilization of the cavity length/modulation frequency is needed for long term operation, especially for high repetition rate mode-locked fiber lasers. In our previous work[30], a simple feedback control is implemented by using kHz electronics with computer monitoring. The laser can stably operate for hours with the stabilization schemes implemented. This is another merit of the ASM soliton lasers since the typical synchronous mode-locked fiber lasers at the high repetition rate will need high speed electronics to stabilize the laser.

On the other hand, at a lower repetition rate, the cavity frequency drift $<|\Delta\Omega_{lim}|_{max}$, so that the operation regime of the fiber lasers could remain in ASM for sufficient time. In this way, no stabilization schemes are needed. In reality, indeed, C. R. Doerr *et al.* have shown this[23]. Another possible approach is to find new kinds of fibers with high dispersion and high gain, and then the total cavity length could be reduced considerably leading to considerable reduction on the frequency drift of the harmonic cavity components.

To conclude, the ASM mechanism provides a new kind of stabilization scheme which doesn't need high speed electronics to implement the feedback control loop as in typical synchronous mode-locking. At the low repetition rate, even no additional stabilization scheme is needed as long as the frequency drift of the cavity harmonic component remains within a certain range. At the high repetition rate, some

stabilization scheme is needed due to larger drifts in higher harmonics.

3.6 Discussions

From our experimental results it is proved that ASM is indeed a viable method for ultra-short pulse generation, especially at high repetition rates. The economic feedback stabilization also shows its additional advantage. The results at 40 GHz can still be improved by adding more dispersion so that the noise can be dispersed out of the soliton more efficiently. This idea is from the observation described in the next paragraph.

The results shown in section 3.2, 3.3 are obtained from the same cavity with the same dispersion and nonlinearity. In an attempt to generate 10 GHz pulse trains, different lengths of single mode fibers were used. When the relative length of SMF to that of EDF was longer, the required pump power was close to our maximum available power and the SMSR was greater than 70 dB. As the relative length of SMF was cut shorter, the required pump power was reduced but with the reduced SMSR (<40 dB) at 10GHz. For this laser cavity, as the modulation frequency raised to 20 and 30 GHz, the SMSR could reach >40dB. This observation seems to support the validity of equation (2.60): the required gain for noises is greater than that for solitons. Higher dispersion and higher modulation frequency could lead to better SMSR.

However, it's known that the net gain is always negative for lasers at the steady state. The sign in equation (2.60) shall be reversed. Furthermore, what is observed in experiments seems to be in contradiction with this negative net gain idea. Therefore, in addition to the requirement for the net gains leading to equation (2.60), it seems that something is to be reconsidered.

To resolve this, if the values in left-hand-side and right-hand-side of equation (2.60) were absolute values, there would be no contradiction. Even so, the validity of

these absolute values needs to be confirmed. There are still plenty of interesting questions to find behind this argument.

In the experiments, when the laser is mode-locked asynchronously at some wavelength, we attempt to change the lasing wavelength by slightly tuning the center wavelength through the tunable band-pass filter with necessary adjustment of the modulation frequency. It turns out that not in all of the tunable range of the wavelengths does the laser stay mode-locked. At some wavelengths the optical spectrum becomes asymmetric. It might be the parasitic filtering effect that causes this phenomenon. This still needs further investigation.

In this thesis, another question of interest is that whether APM is necessary for ASM. In our experiments, when the polarizer hadn't been placed at the input end of the EO phase modulator, the APM didn't occur when the polarization state was adjusted, and neither did ASM. With a polarizer, ASM as well as APM occurred. One question arises that whether this polarizer in cooperation of other cavity elements gives any mechanisms other than APM to make ASM possible or it is just APM? All of these questions are worthwhile to be investigated for a deeper understanding.

Chapter 4

Numerical Simulations

4.1 The master equation and numerical method

To simulate the dynamics of the mode-locked lasers, an average model presented in chapter 2 is used. Presented below, for convenience, is the master equation with the APM effect in the process of pulse generation:

$$T_R \frac{\partial}{\partial T} a = \left\{ (g-l) + \left[\left(\frac{1}{\Omega_f} \right)^2 + jD \right] \frac{\partial^2}{\partial t^2} + jM \cos\left(\Omega_M (t + \Delta T(T)) \right) + (\gamma - j\delta) |a|^2 \right\} a$$

(4.1)

where
$$\Delta T(T) = -\frac{\Omega_H - \Omega_M}{\Omega_M} T$$
(4.2)

$$\left(\frac{1}{\Omega_f} \right)^2 = g \left(\frac{1}{\Omega_g} \right)^2 + \left(\frac{1}{\Omega_{filter}} \right)^2$$
(4.3)

In this model, a band-pass filter is also introduced in the laser cavity for accounting the effect of the tunable band-pass filter used in the experiments. The numerical method is the standard split-step Fourier transform used in pulse propagation problems. The formulation is described in the following paragraph:
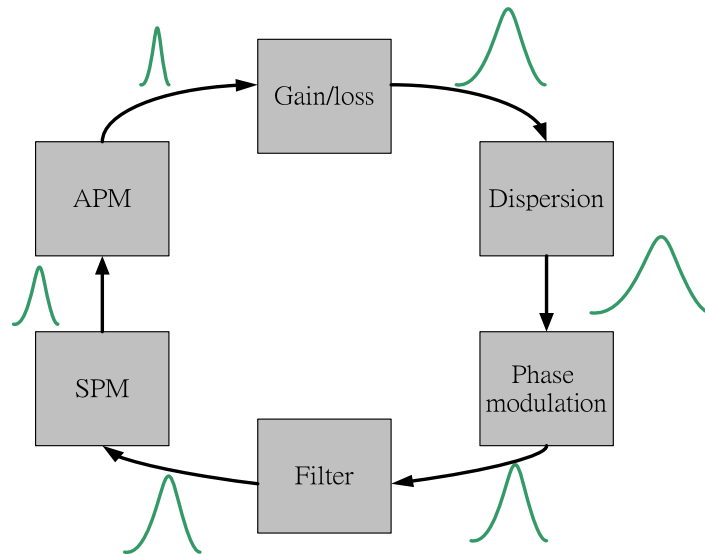

Fig.4.1 An average lumped model

The RHS of equation (4.1) can be re-arranged into two groups of operators by deciding whether it is a constant operator at that time or not. The resultant pulse evolution equation can be written as:

$$\frac{\partial}{\partial T} a = (\hat{A} + \hat{B})a \tag{4.4}$$

where

$$\hat{A} \equiv \frac{1}{T_R} \left\{ \left(\left(\frac{1}{\Omega_f} \right)^2 + jD \right) \frac{\partial^2}{\partial t^2} \right\} \tag{4.5}$$

and

$$\hat{B} \equiv \frac{1}{T_R} \left\{ jM \cos \left(\Omega_M \left(t + \Delta T(T) \right) \right) + \left(g - l \right) + \left(\gamma - j\delta \right) |a|^2 \right\} \tag{4.6}$$

$\hat{B}$ is the constant operator at some time while $\hat{A}$ is a differential operator. After some small propagation time the resulting pulse is:

$$a_{m+1} \cong \exp \left(A \frac{\Delta T}{2} \right) \cdot \exp \left(\hat{B}_m \Delta T \right) \cdot \exp \left(\hat{A} \frac{\Delta T}{2} \right) a_m, m = 0,1,2... \tag{4.7}$$

For each iteration, equation (4.7) is evaluated in a split-step manner: first, apply the $\hat{A}$ operator in the frequency domain with the Fourier transform pair, $\frac{d}{dt} \rightarrow -j\omega$, and then transforming back to the time domain; second, directly apply the $\hat{B}$ operator in the time domain; the last step is the same as the first step. The programming plateform is the Matlab software. For the correctness of the simulation, an accurate or at least reasonable estimation of the parameters is necessary. The values and units used in the simulation are listed in the table (The wavelength is 1560 nm). Also, the absorbing boundary condition is implemented with a parabolic loss term within the window to prevent reflected waves from interfering with the pulse.

Table 4.1 Estimated values of parameters

Item	Value	Unit
T_R	150	**Ns**
Harmonic[th]	4500/6000	
SMF		
β_2	-0.02328	**ps²/m**
δ	0.00122	**W⁻¹/m**
EDF		
β_2	0.05164	**ps²/m**
δ	0.00629	**W⁻¹/m**
I_{sat}	70.39949	**MJ/m²s**
$\Delta\lambda_g$	30	**nm**
Tunable Filter		
$\Delta\lambda_f$	12.5	nm
Phase Modulator		
M	0.3~0.5	radian
Ω_M	30 / 40	GHz
APM		
γ	0.0069 /	**W⁻¹**

4.2 The simulation of ASM

In this section, numerical simulation is performed to see if the resulting pulse properties are identical to those predicted by the analytical theory in a qualitative manner. To do so, accurate parameter or at least reasonable estimation is required. To do this, some of the values of the parameters are obtained from the experimental measurement or estimation. However, in most of the cases these values in simulation don't match exactly to those of the experiments and the resulting pulse properties are very sensitive to the set of parameters. Here, a qualitative instead of quantitative comparison is attempted.

4.2.1 Asynchronous mode-locking at 30 GHz

The following figures show the steady state pulse shape and the evolution with time when the frequency detuning is 40 kHz. The resultant pulse is 0.5*1.763=0.881 ps in width with a soliton pulse shape. The soliton area theorem is satisfied, $\sqrt{\dfrac{-2D}{\delta}} \cong A_o\tau = 1.15$. The output power is 20mW from a 10% coupler. A simulation period of 167 round trips is obtained. The estimated values from table 4.1 are listed bellow:

Table 4.2. Values of parameters*

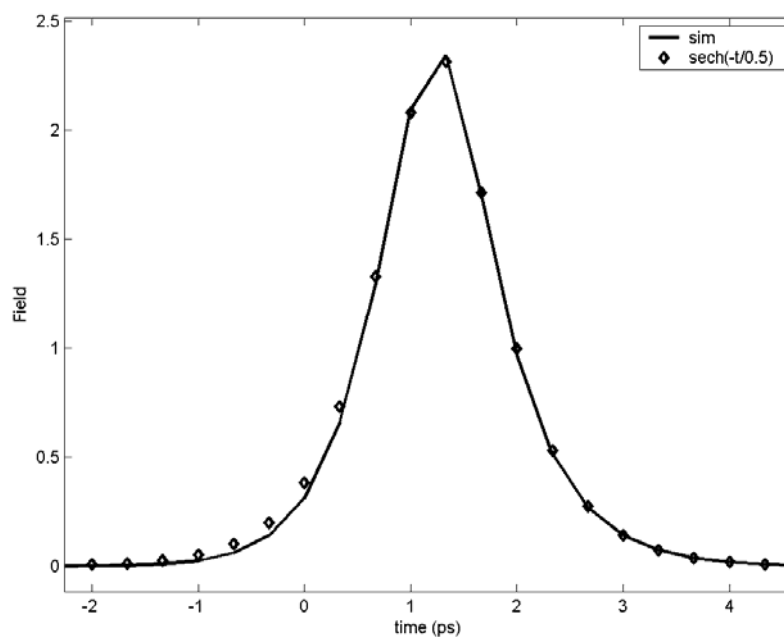| Round trip times	150	ns
Dispersion	-0.02	ps^2
Kerr	0.03	W^{-1}
Gain bandwidth	3.75	THz
Filter bandwidth	1.56	THz
Modulation index	0.2	
Detuning frequency	40	kHz
APM	0.011	W^{-1}

Fig.4.2 The resultant pulse shape is a 0.5-ps sech soliton pulse.

*Note: values are not exactly the same as those in the experiments
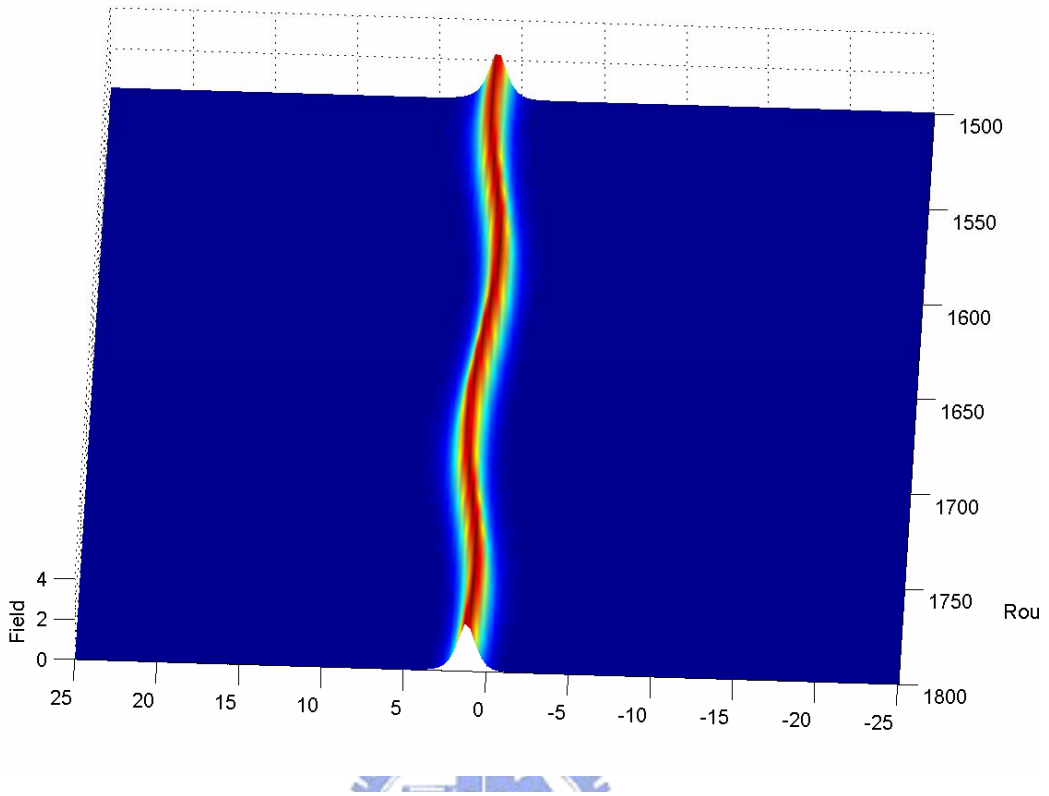
Fig.4.3 The pulse evolution with a period of 167 round-trips from
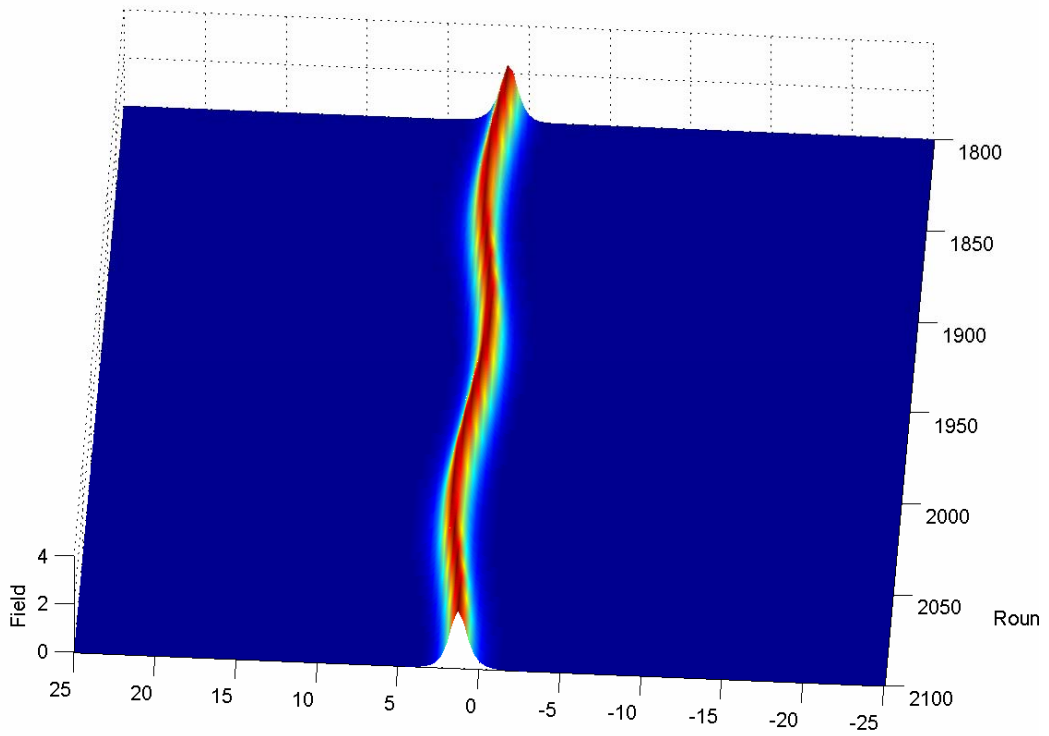
1500 to 1800 round-trip times.

Fig.4.4   The pulse evolution with a period of 167 round-trips from

1800 to 2100 round-trip times.

50

4.2.2 Asynchronous mode-locking at 40 GHz

When the modulation frequency is raised up to 40 GHz with a frequency detuning of 40 kHz(166 round-trip period), the pulse-width is shortened to 793 fs. The output power is 27 mW from a 10% coupler. The gain is raised to provide larger cavity powers for supporting more pulses. The values of the other parameters are all the same as those at 30 GHz. The table of values is repeated here for convenience.

Table 4.2. Values of parameters

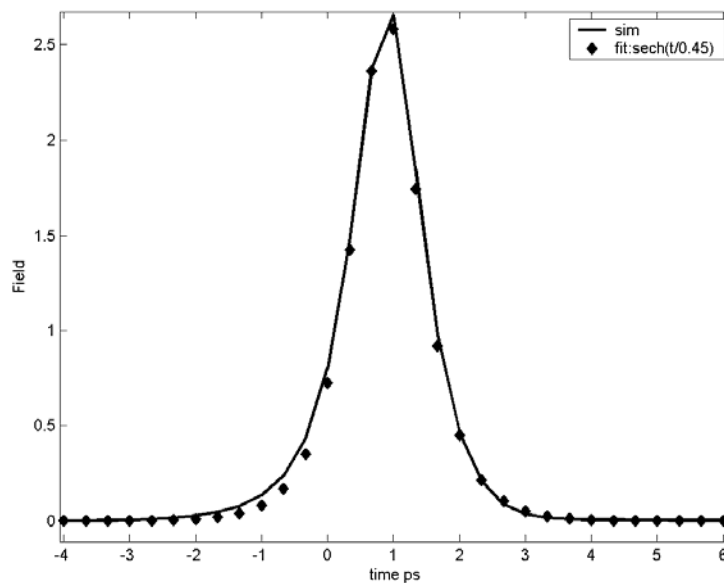| Round trip times	150	ns
Dispersion	-0.02	ps^2
Kerr	0.03	W^{-1}
Gain bandwidth	3.75	THz
Filter bandwidth	1.56	THz
Modulation index	0.2	
Detuning frequency	40	kHz
APM	0.011 W^{-1}	

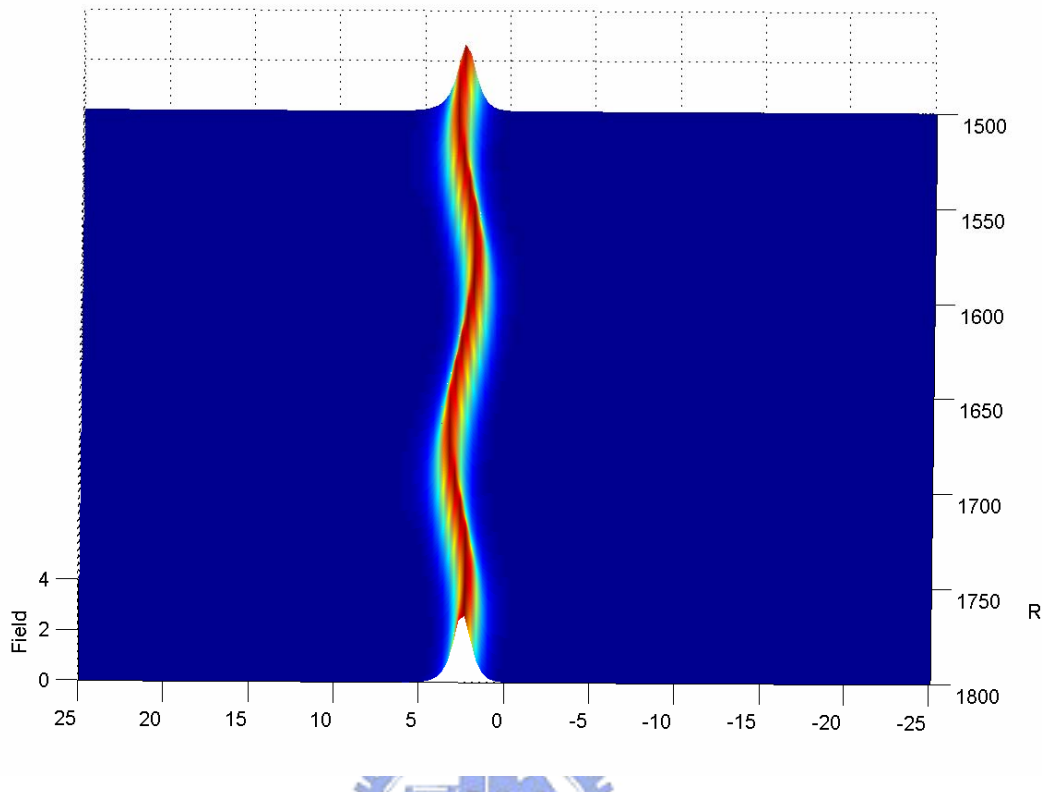Fig.4.5 The resultant pulse shape is a 0.45-ps sech soliton pulse.

Fig.4.6   The pulse evolution with a period of 167 round-trips from
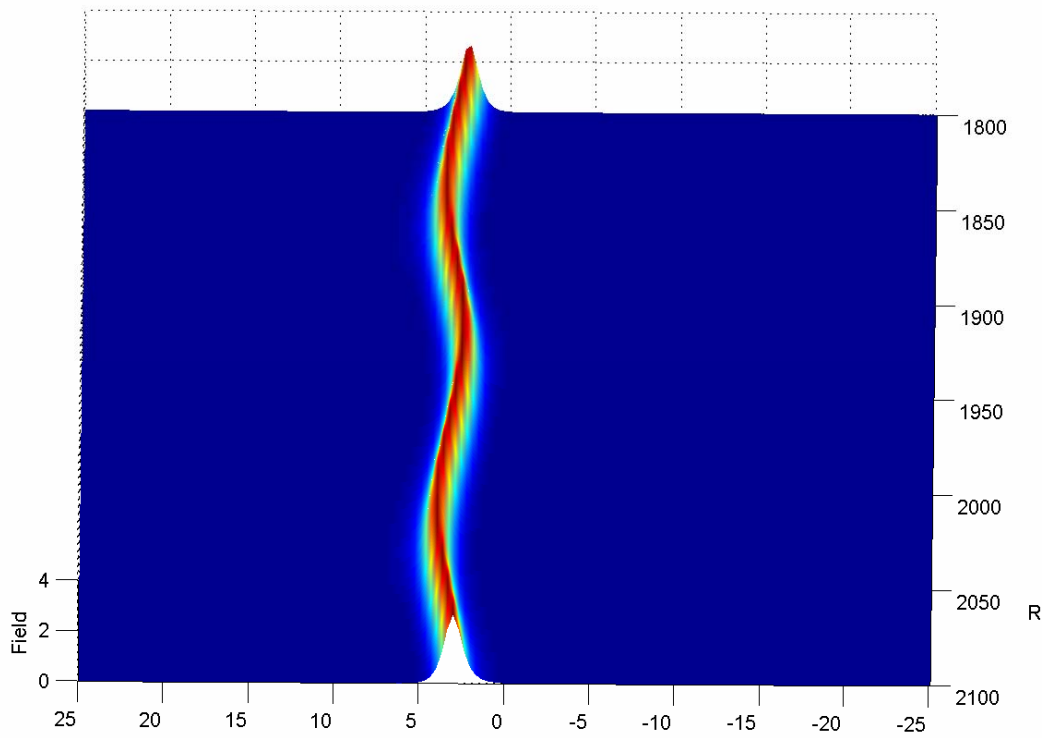
1800 to 2100 round-trip times.

Fig.4.7   The pulse evolution with a period of 167 round-trips from

1800 to 2100 round-trip times.

4.3 Discussion

In this section, the impacts from various parameters on the pulse properties at the steady state of asynchronous mode-locking are discussed in a qualitative manner. Only one parameter is changed at one time with the others fixed to see how the result changes. The noise isn't considered in the simulation.

● **Phase modulator**

The effects of the modulation index are explored without APM participating in the process. The values are listed in the table. The modulation index is varied from 0.6 to 1.5 in this case. Before doing the simulation, it can be known from the equations (2.19) and (3.58-61) that the pulse width, frequency shift, noise-cleanup effect, and the maxima detuning range are related to the modulation index.

Table 4.3 values of parameters

Item	Value	Unit
E_{sat}	400	**pJ**
Δf_g	3.75	**THz**
g_0	7	
Loss	2	
Δf_{filter}	1.56	THz
M	0.6-1.5	
f_m	10	GHz
Δf	20	kHz
harmonic	50	
T_R	50	ns
D	-0.05	**ps^2**
δ	0.01	**W^{-1}**
γ	0	**W^{-1}**

Figures 4.8-10 show the resultant pulse evolution, the cavity power relaxation and the pulse-width when M=0.8. Figure 4.8 also shows that the slow modulation period is 1000 round-trips, which corresponds to 20 kHz frequency deviation.
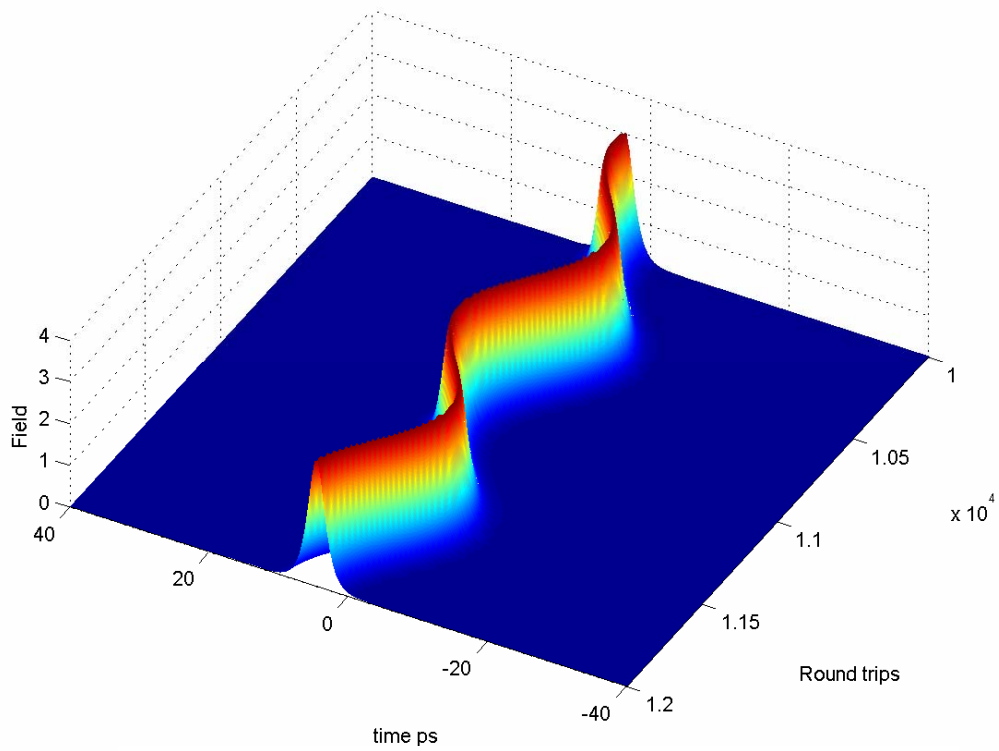
Fig.4.8   The pulse evolution at 1 GHz with a period of 5000 round-trips
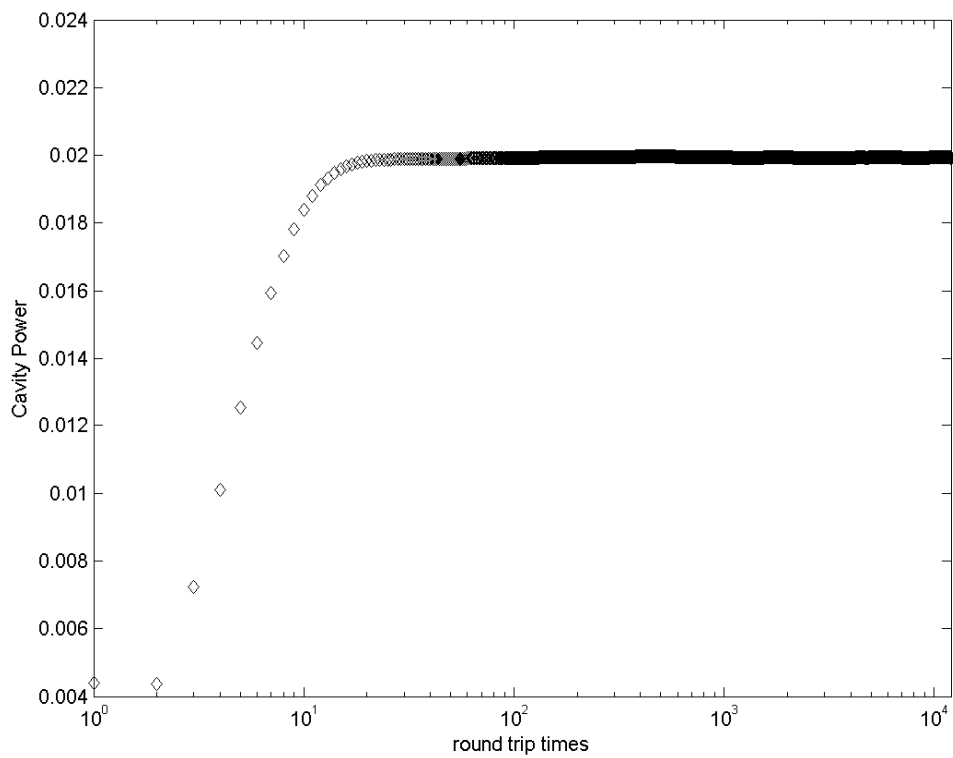
from 10000. to 12000 times, M=0.8.
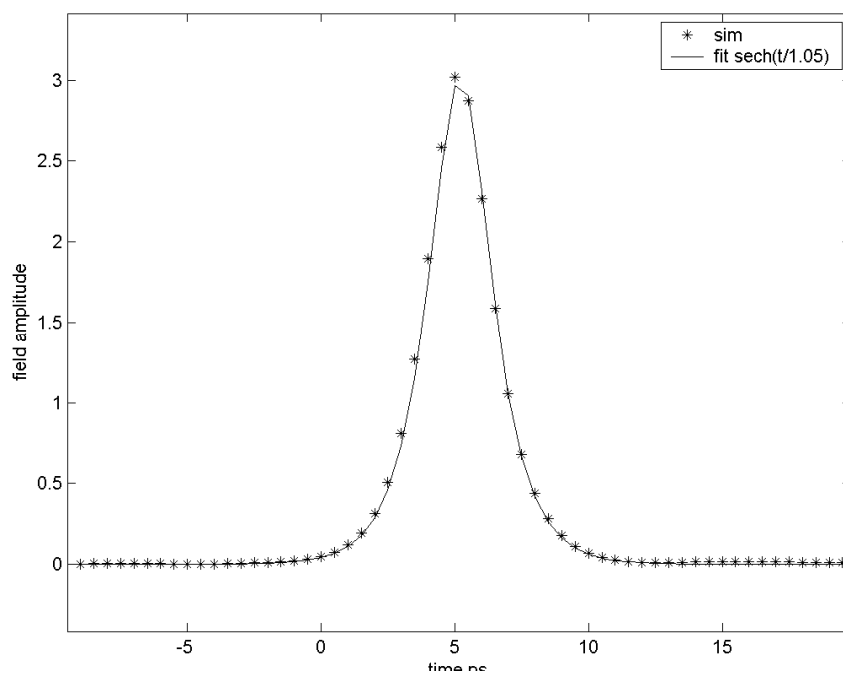

Fig.4.9   The cavity power relaxation.

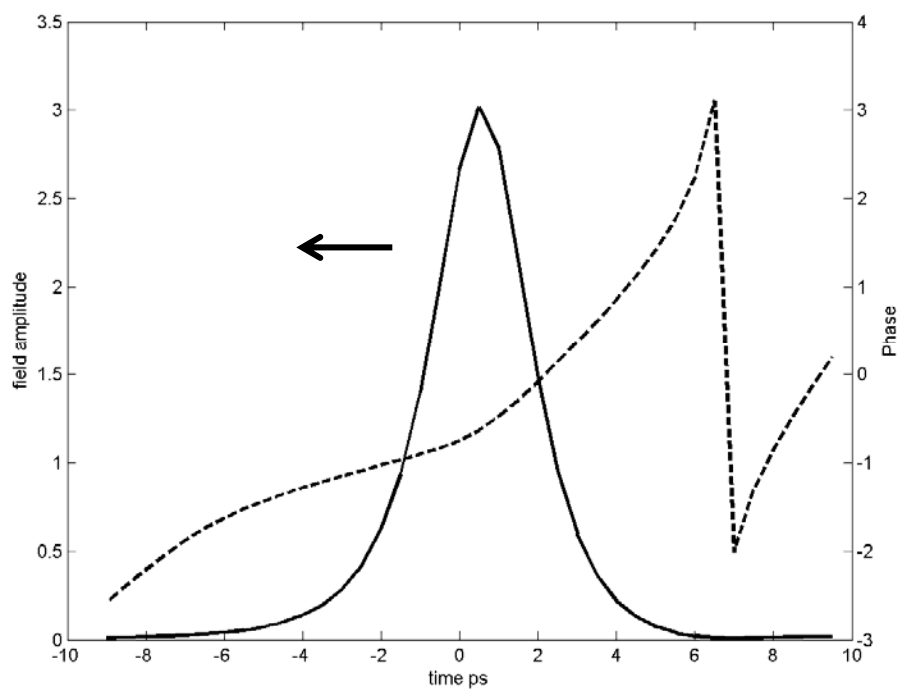Fig.4.10   The resultant 1.78 ps soliton pulse at 1GHz, M=0.8.

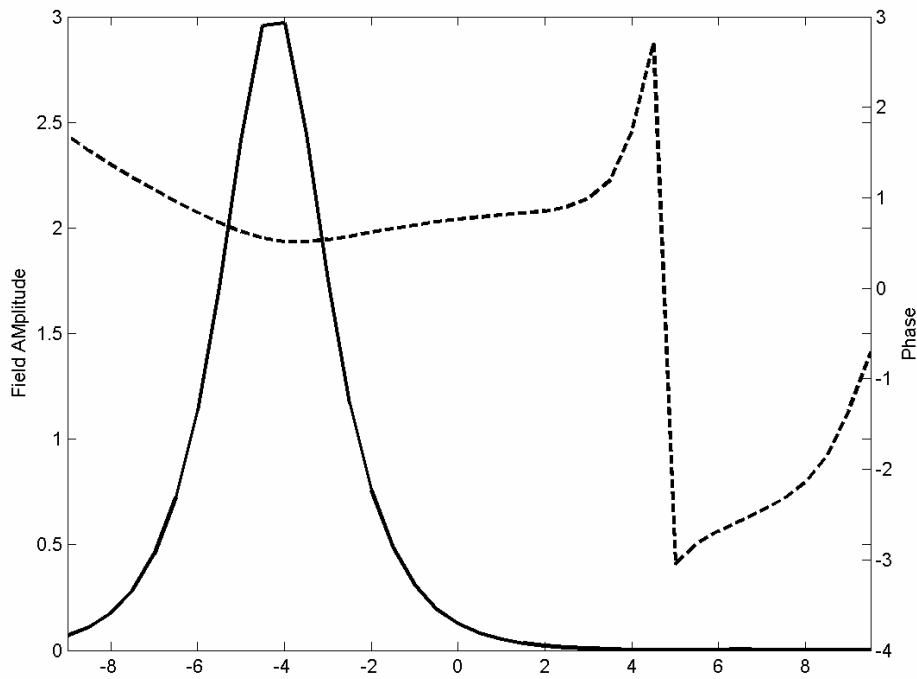Fig.4.11 The phase along the pulse which moves left, M=0.8.

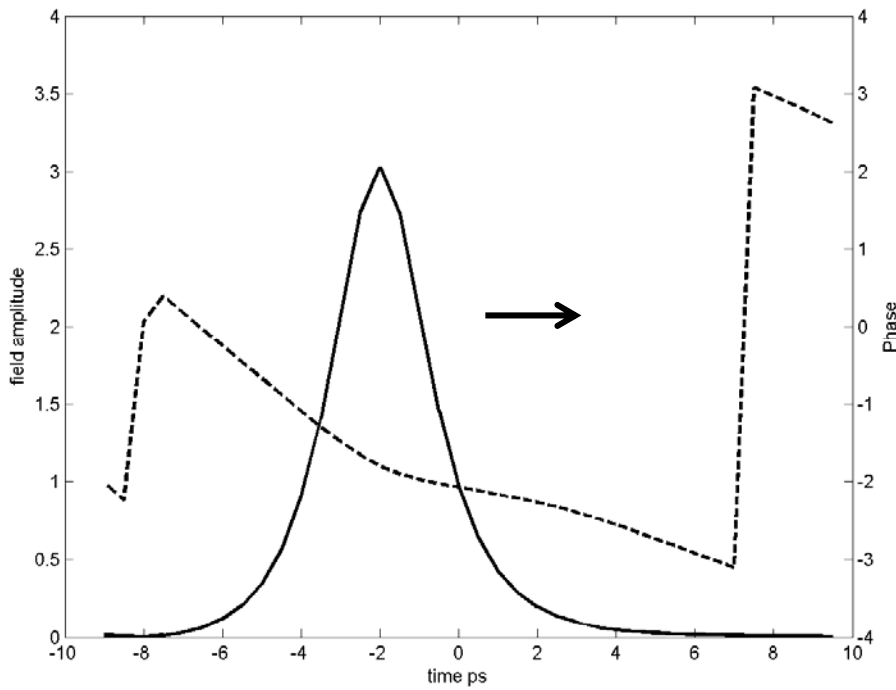Fig.4.12 The phase along the pulse at the left end, M=0.8.

Fig.4.13 The phase along the pulse moving right, M=0.8.

Figures 4.11-13 also show the phases along the pulses at some time spots. It is found that the soliton is of a little chirp from the quadratic phase curve. The slope of the phase also shows that the frequency of the pulse is shifted in a periodic manner which in turns leads to pulse timing variation. The peak-to-peak timing variation is about 9.77 ps.

The next figure shows the situation after thousands of round trips when the modulation index is changed to 0.6 at 12000 round-trip. It turns out that the pulse is no longer stable. The pulse sheds off continuous waves which get amplified in turns.
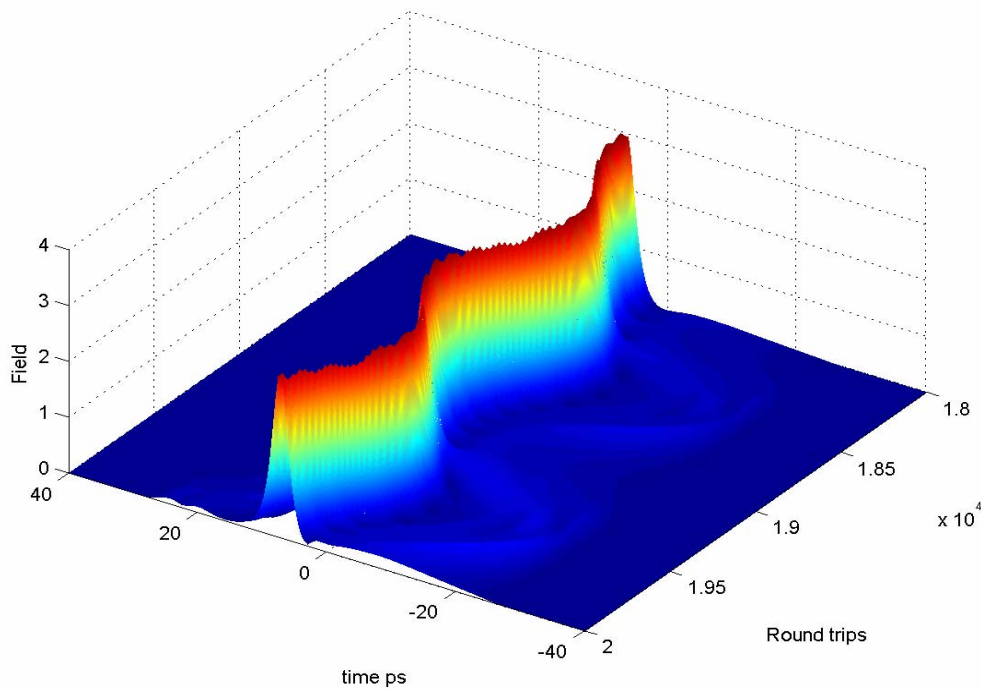

Fig.4.14   The pulse evolution at 1 GHz with a period of 18000
round-trips from 18000. to 20000 times, M=0.6.

When the modulation index is changed to 1.2, the peak-to-peak timing variation becomes larger, 15 ps, and there are less continuous waves. The resultant pulse width is almost unchanged. It may be because the pulse-width is shortened by soliton compression and is already beyond the Kuizenga–Seigman limit, 11.6 ps, at 1GHz. The following figures show the results.
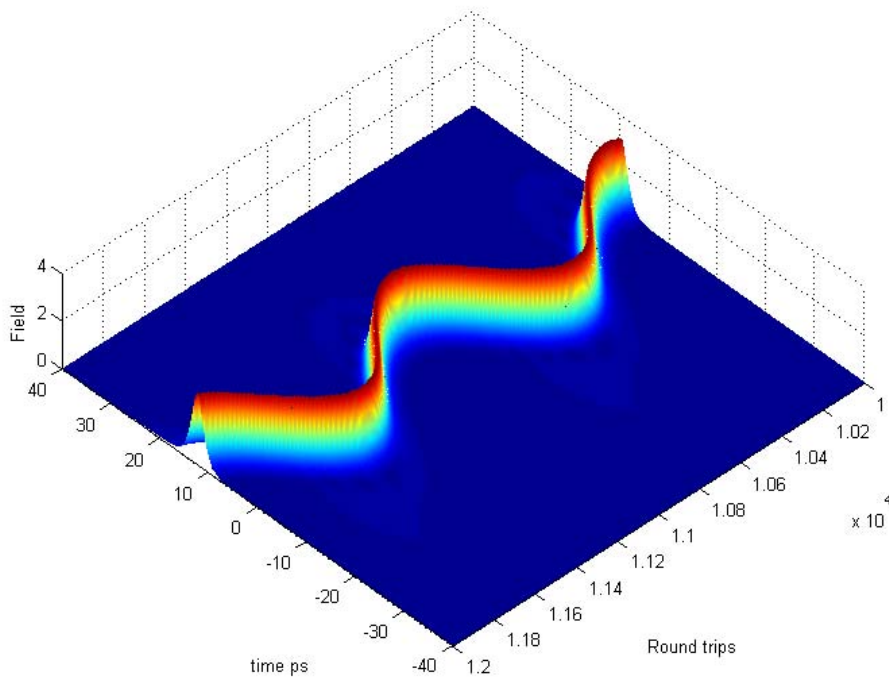
Fig. 4.15 The pulse evolution at 1 GHz with a period of 18000 round-trips
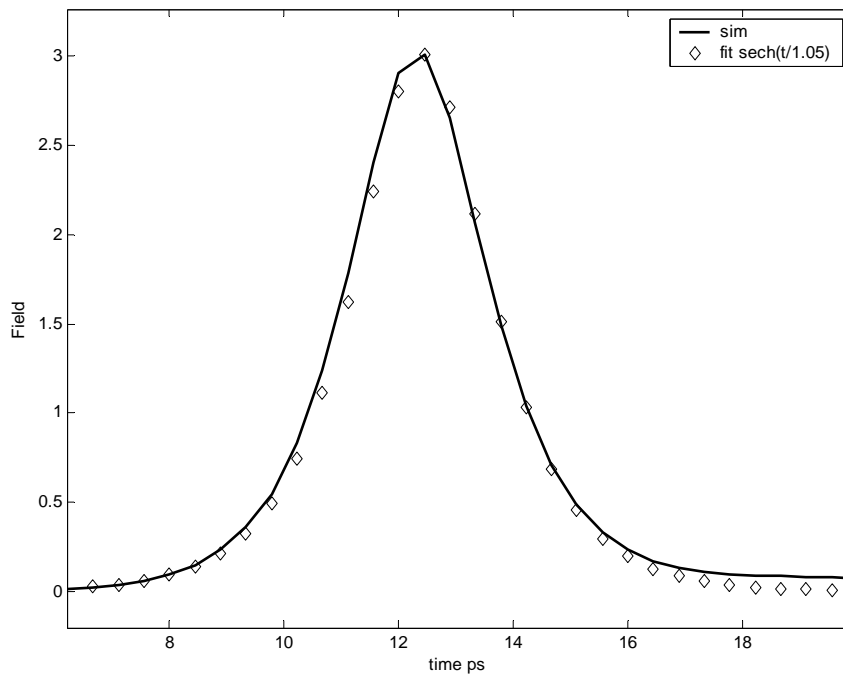
from 10000. to 12000 times, M=1.2.

Fig.4.16   The resultant pulse when M=1.2.

The changes in the peak-to-peak timing variation with respect to the modulation index are plotted in the figure 4.17. It is found that the peak-to-peak timing variation changes linearly with the modulation index. Figure 4.18 shows the resultant pulse width with respect to the modulation index. The pulse width is almost the same for different indices. For the modulation index = 1.6, the pulse shape is of Gaussian instead of sech. This may imply that there is a condition under which the pulse-width remains unchanged regardless of the modulation index.
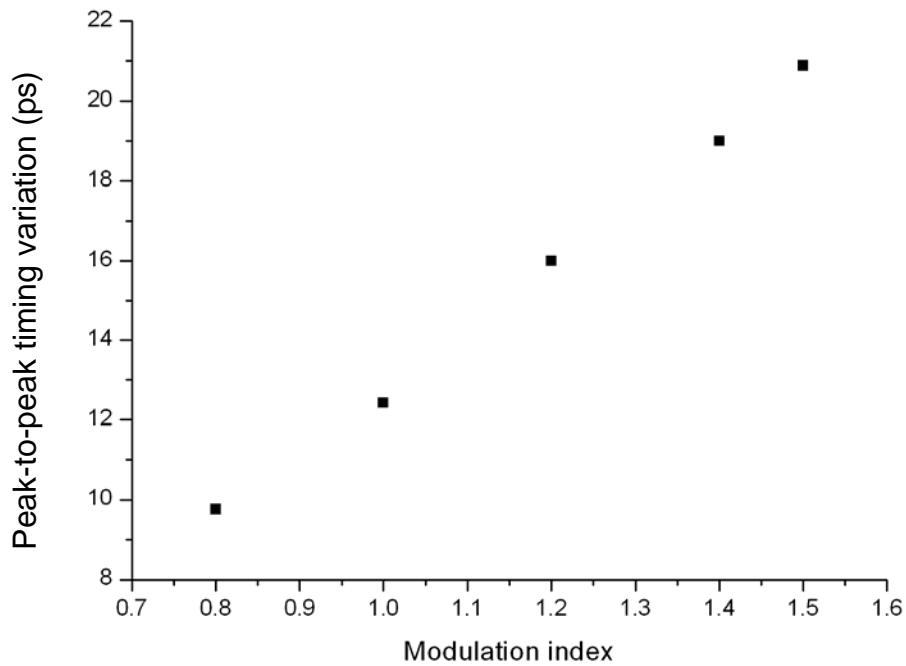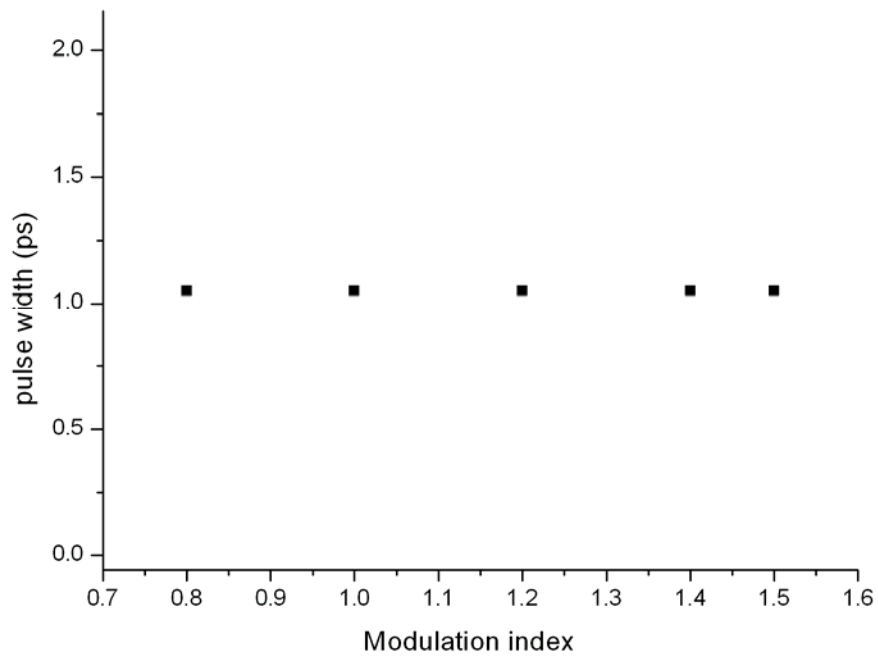

Fig. 4.17 The timing variation changes with M

Fig.4.18 The resultant pulse remains invariant for a range of M.
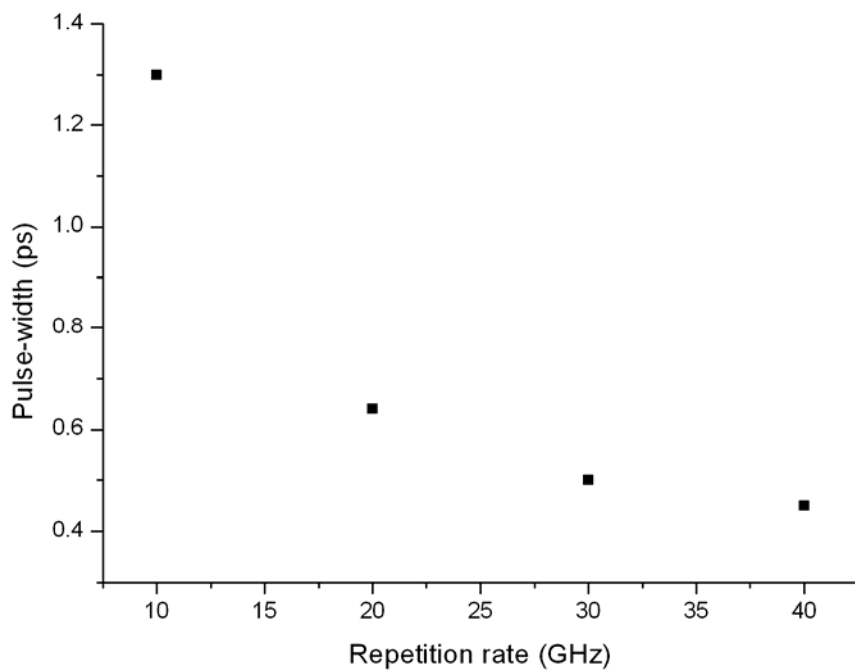

Fig.4.19 The resultant pulse-width changes inverse-proportionally with the

modulation frequency.
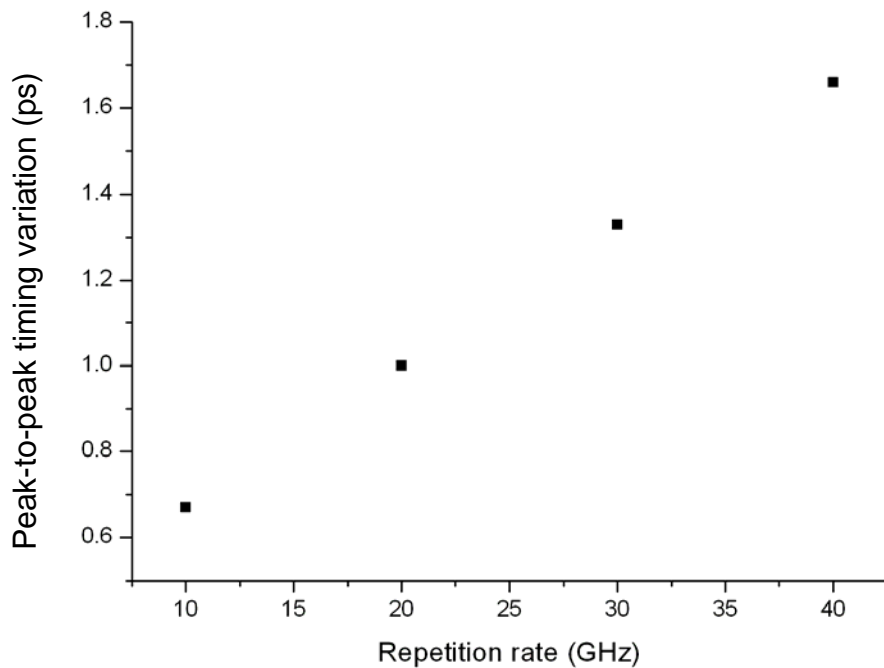
Fig.4.20 The peak-to-peak timing variation changes linearly with the modulation
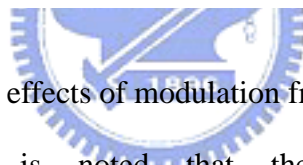
frequency.

Figures 4.19-20 show the effects of modulation frequency on the pulse-width and the timing variation. It is noted that the pulse-width is shortened inverse-proportionally with the modulation frequency. The peak-to-peak timing variation grows linearly with the modulation index.

To verify whether these results are reasonable or not, we can refer to the timing variation derived from the soliton perturbation theory, equations (2.57-59); the timing variation is indeed proportional to the modulation index and modulation frequency. The results of the pulse-width maybe right and need experimental and theoretical verification.

Notes: the simulations results, figures 17 and 19, of the effects of the modulation frequency uses the values listed in table 4.2 instead of table 4.3. The values in table 4.3 are used to explore the effects of the modulation index, the

dispersion and the APM.

In the following sections, the effects of the dispersion and the APM are simulated. It can also be verified that the timing variation is proportional to the dispersion. Experimental and theoretical verifications are needed to check the effects of the dispersion on the pulse-width and the effects of APM.

● Dispersion

This section shows the effects of dispersion on the pulse-width and the peak-to-peak timing variation. The timing variation gets larger when cavity dispersion gets larger. The trend is shown in the following figure. It's known that the time delay due to the frequency shift is proportional to dispersion. The timing variation shown here is not assured to change in a linear or quadratic form. But the general trend seems to be reasonable by considering the frequency-shift-induced time delay.
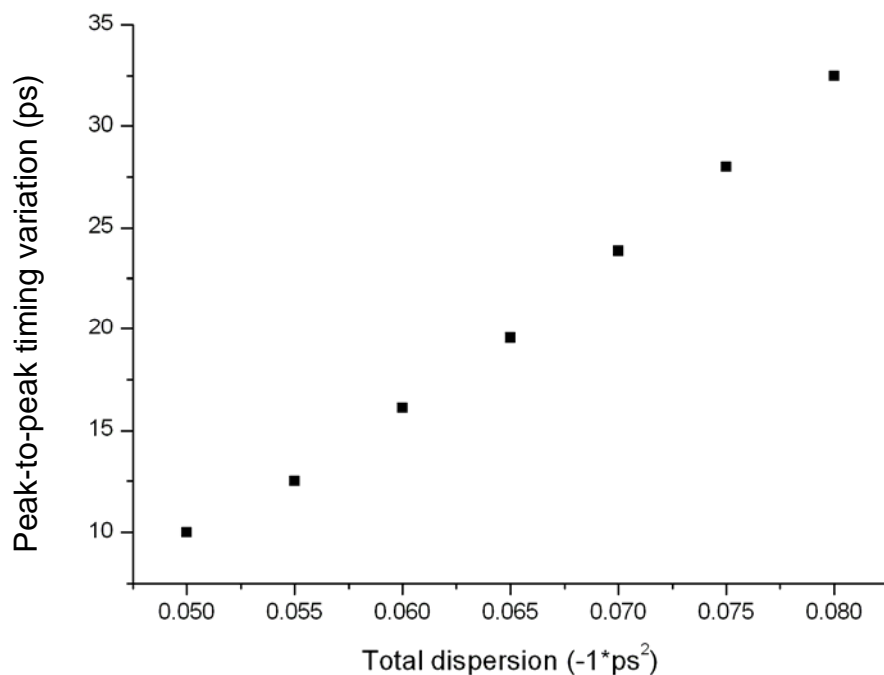
Fig.4.21 The peak-to-peak timing variation changes with dispersion.
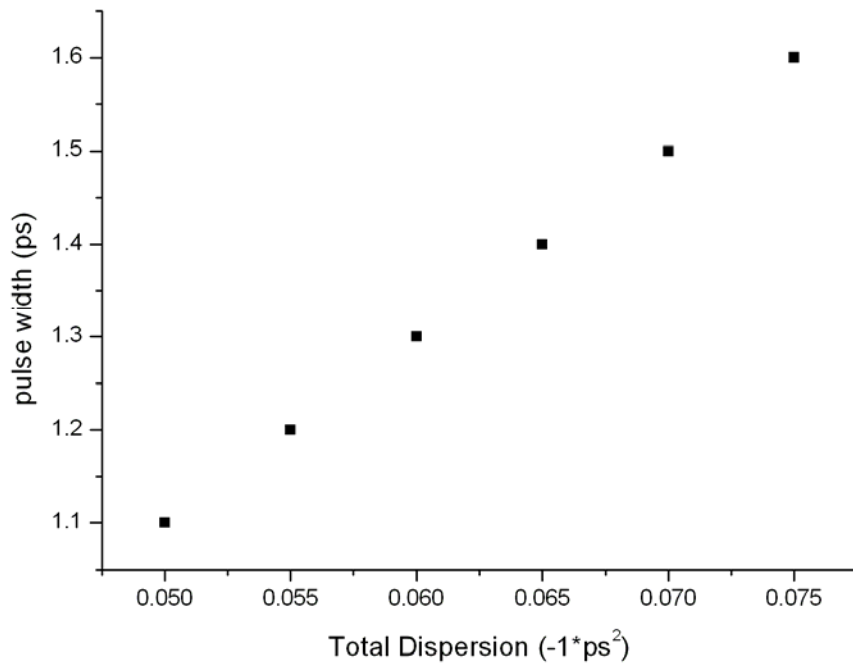
Fig.4.22 The resultant pulse width changes linearly with dispersion.

The resultant pulse-width seems to be in a linear relation with respect to the dispersion from the simulation results. With larger dispersion the pulse width is also wider. Experiments are needed to measure the timing variation and pulse width for further investigation.

● **APM**

The previous discussion doesn't take the APM effects into account. Here, this effect is included by setting $\gamma = 0.005$. The simulation results show that the pulse width and the timing variation are both reduced. The reduced pulse width may be expected since APM can shorten the pulse width nonlinearly. The more interesting result is that the timing variation is also reduced in ASM by APM. The following figures show the simulation results.

Fig.4.23   Timing variation is reduced by APM.

Fig.4.24 The resultant pulse width is reduced by APM.

Chapter 5

Summary and Future Works

5.1 Summary

In this thesis, asynchronous mode-locking is demonstrated to be a viable and economic method for ultra-short pulses generation at 40GHz both in experiments and simulation. In the experiments, the resulting pulse width is 596 fs with SMSR > 40 dB when the detuning frequency is 20 kHz at 30 GHz and 860 fs with the 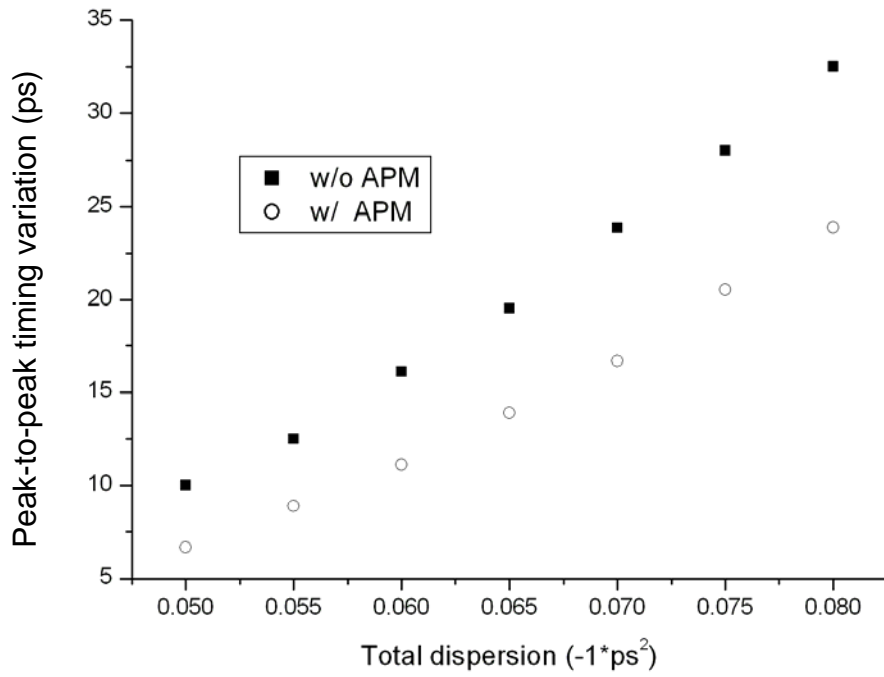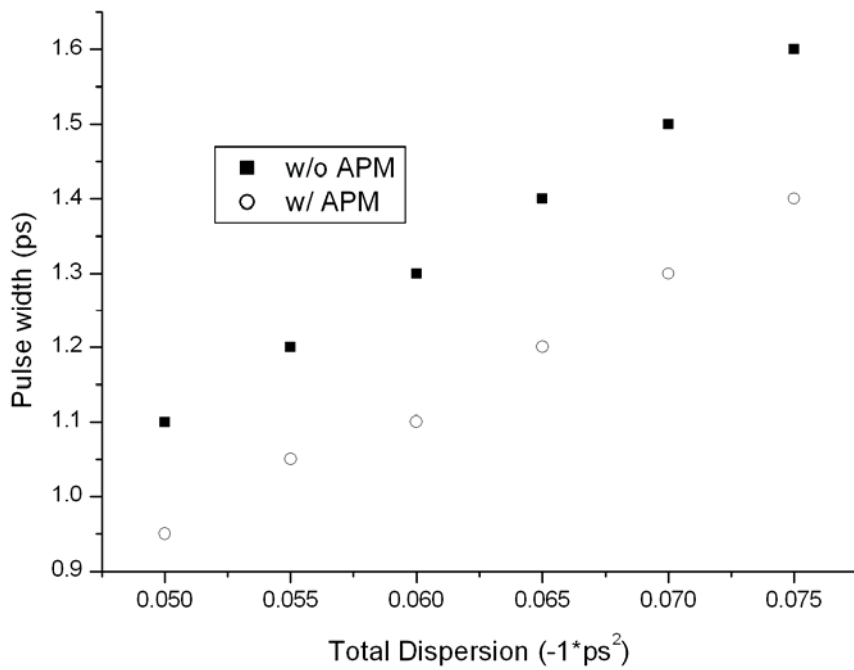same SMSR at 30GHz when the detuning frequency is 30 kHz at 40GHz. In simulation, the results reasonably agree with those from the experiments.

From the results of the simulation and experiments, the effects of the phase modulator in ASM are described in terms of the modulation index and the modulation frequency. In simulation, it seems that the modulation index has a small impact on the pulse-width, because the pulse-width is mainly determined by the soliton effects and is already beyond the Kuizenga–Seigman limit. The peak-to-peak timing variation is larger with the increasing modulation index, which has been confirmed by the perturbation theory.

In the experiments, larger modulation index leads to wider optical spectra but the pulse energy is too small to measure the real pulse width by SHG autocorrelation. The wider optical spectra may be due to the fact that the pulse gets chirped by the phase modulator while the pulse-width remains the same. Future works need to be done to confirm if this is possible by raising the pulse energy for measurement.

As for the modulation frequency, both in experiments and simulation, the pulse width is more shortened by using a higher modulation frequency. Although in this experiments the pulse width is not directly measured, in the previous experiments by C. R. Doerr[23] *et al* and by ours[24], shorter pulse-widths with higher modulation

frequency is observed.
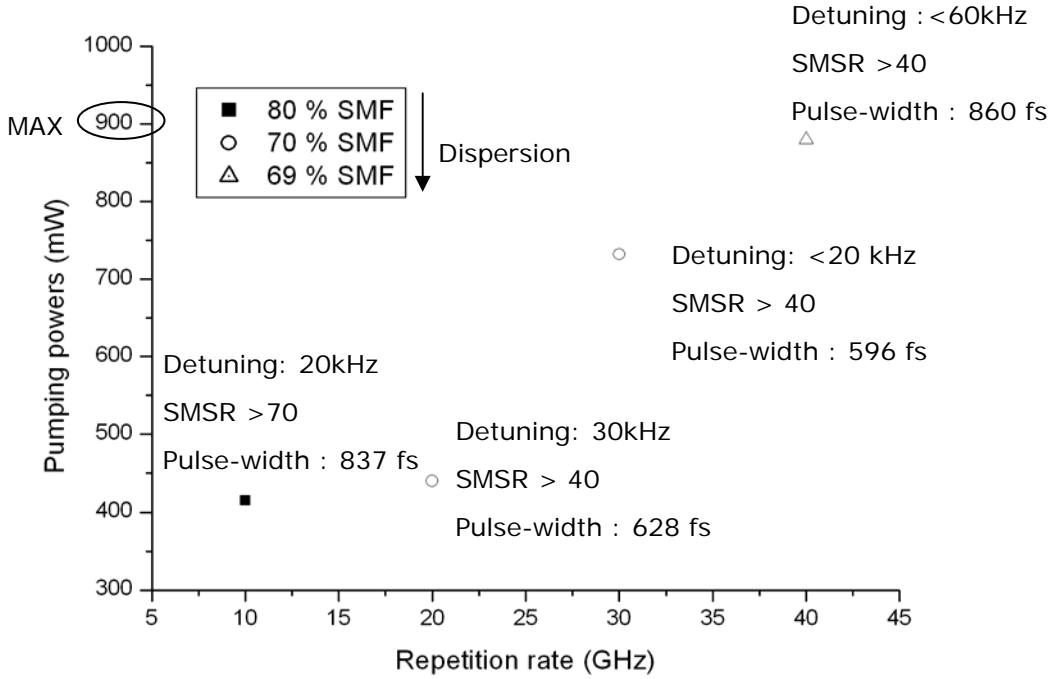
Fig 5.1 A summary of the experimental data.

In simulation, with a larger dispersion the pulse width and the timing variation will grow. The increasing pulse width may be explained by the broadening effect due to dispersion. The increasing timing variation may be due to the fact that the time delay by the frequency shift is proportional to the dispersion. Further investigation may be performed in experiments to confirm these observations. The functional forms for the timing variation and the pulse-width are arranged as follows:

$$\Delta T \propto M, D, f\left(\Omega_M, \frac{1}{\gamma}\right) \tag{5.1}$$

$$\tau_s \propto D, f\left(\frac{1}{\Omega_M}, \frac{1}{\gamma}\right) \neq f(M) \tag{5.2}$$

The effects of the APM in ASM are investigated by simulation. The pulse width is shorter as expected, and the timing variation is reduced, too. This smaller timing variation due to APM is an interesting phenomenon and may need further investigation. Although in simulation it is still possible for pulses to form without

66

APM, in experiments no ASM is observed without APM.

5.2 Future Work

● Theoretical work

The effects of the phase modulator in ASM need an explicit analytical expression for accurate estimation. Future work may include expanding the phase modulation term to second order in the master equation and substituting the Sech ansatz into it to find a more analytical solution. In this way, the effects from various parameters on the solution may also be studied.

● Experimental work

In experiments, the relative length of SMF to that of Erbium-doped fiber plays an important role, since the resulting soliton energy is determined by the net cavity dispersion and nonlinearity. Once the relative length is determined, the cavity dispersion as well as the cavity nonlinearity is determined. Usually, it is preferable that there are more degrees of freedom to operate. If the cavity dispersion and nonlinearity can be chosen independently, it is possible to lower the soliton energy while maintaining the cavity dispersion by just increasing the cavity nonlinearity. To do this, certain types of fiber-compatible devices are desirable. For example, high nonlinearity fibers which have almost zero dispersion around 1550 nm are quite desirable. In this way, higher SMSR and lower required pumping power can be achieved and we can perform some experiments to make sure if the dispersion really helps improving the SMSR.

In addition, in ASM fiber lasers a wide band width filter is needed for shorter pulses and such a suitable wide band filter may not be easy to get and also expensive. An alternative choice is to use a Sagnac loop interferometer based on the polarization maintaining fiber as a wide band filter. Attentions must be paid to the reflection

effects of the devices, because ASE noises will be induced when there is a gain medium between the devices which reflect lights. It is encouraged to invent or find new kinds of new devices depending on the applications. For example, a special material called "photonic crystal" is attracting great attentions for its diversity.

Since the power inside the cavity is approximately 200~300 mW depending on the gain medium and pumping powers, the pulse energy is smaller when repetition rate is higher. It's not easy to measure the pulse-width by SHG autocorrelation. New measurement techniques and distortion-free amplification techniques are needed.

The frequency shifts of the soliton are also needed to be measured. The main difficulty is that the frequency component at 20~40 kHz on RF spectra includes the contributions from the timing variation and the frequency shifts. These two effects need to be separated by some methods.

● **Simulation Work**

In doing simulations, it is always a good idea to find a more efficient algorithm, no matter in memory space or computation time. In the case of ASM, since the pulse moves within the computation window, if the window could move accordingly, computation time would be saved due to reduced redundant part of the computation window. Especially, the timing variation grows with a higher repetition rate. Therefore, a moving computation window is needed. Furthermore, with the growing computation ability of computers form years to years, a more efficient algorithm is always desired.

In the process of doing simulation, we've found that the time spot on which APM occurs is important; if there are considerable continuum waves before the effects of APM get greater, it is possible to form pulses from these continuum waves. Otherwise, APM acts as a noise cleaner and a pulse shaper. The role of APM in ASM

is still needed to be explored and defined. Also, the noise sources can be added to the equation for a simulation of a real system.

Notes

Most parts of this thesis put the emphasis on the steady state of the laser system. In fact, the initial situation of lasers which depends on the noise effects[32], and the operation conditions has an influence on the dynamics of lasers. This is a challenging research topic.

References

[1] Dirk J. Kuizenga and A. E. Siegman, "FM and AM Mode Locking of the homogeneous Laser - Part I: Theory" IEEE J. Quantum Electronics, vol. 6, no. **11**, pp. 694-708, 1970.

[2] Hermann A. Haus, "Mode-locking of Lasers", IEEE J. Quantum Electronics, vol. 6, no. **6**, pp. 1173-1185, 2000.

[3] Hermann A. Haus, David J. Jones, Erich P. Ippen, and William s. Wong, "Theory of Soliton Stability in Asynchronous Mode-locking", IEEE J. Lightwave Technology, vol. 14, no. **4**, pp. 622-627, 1996.

[4] A.B. Grudinin, D.J. Richardson and D.N. Payne, "Passive harmonic mode-locking of a fibre soliton ring laser", IEEE J. Electronics Letter, vol. 29, no. **21**, pp. 1860-1861, 1993.

[5] Herman A. Haus, "Theory of mode locking with a fast saturable absorber", J. Applied Physics, vol.46, no.**7,** pp. 3049-3058, 1975.

[6] Hermann A. Haus, "Theory of Mode Locking with a Slow Saturable Absorber", IEEE J. Quantum Electronics, vol.11, no. **9**, pp. 736-746, 1975.

[7] G. T. Harvey and L. F. Mollenauer, "Harmonically mode-locked fiber ring laser with an internal Fabry-Perot stabilizer for soliton transmission", Optics Letters, vol. 18, no. **2,** pp. 107-, 1993.

[8] M. Nakazawa, K. Tamura and E. Yoshida, "Supermode noise suppression in a harmonically mode-locked fibre laser by selfphase modulation and spectral filtering", Electronics Letters, vol. 32, no. **5**, pp. 461-, 1996.

[9] L.E. Nelson, D.J. Jones, K. Tamura, H.A. Haus, E.P. Ippen, "Ultrashort-pulse fiber ring lasers", Apply Physics B, vol. 65, no. **2**, pp. 277–294, 1997.

[10] H. A. Haus, J. G. Fujimoto, and E. P. Ippen, "Structures for additive pulse mode

locking", J. Optical Society of America B, vol. 8, no. **10**, pp.2068-, 1991.

[11] H. A. Haus, E. P. Ippen, and K. Tamura, "Additive-Pulse Modelocking in Fiber Lasers", IEEE J. Quantum Electronics, vol. 30, no. **1**, pp. 200-208, 1994.

[12] L. F. Mollenauer and R. H. Stolen, "The soliton laser", Optics Letters, vol. 9, no. **1**, pp. 13-, 1984.

[13] J. Mark, L. Y. Liu, K. L. Hall, H. A. Haus, and E. P. Ippen, "Femtosecond pulse generation in a laser with a nonlinear external resonator", Optics Letters, vol. 14, no. **1**, pp. 48-, 1989.

[14] Becker, Olsson, Simpson, "Erbium-Doped Fiber Amplifiers", Academic Press.

[15] H. A. Haus and Y. Silberberg, "Laser Mode Locking with Addition of Nonliner Index," IEEE J. Quantum Electronics, vol. 22, no. 2, pp. 325-331, 1986.

[16] A. Dunlop, W. Firth, and E. Wright, "Pulse shapes and stability in Kerr and Active Mode-Locking (KAML)", Optics Express, vol. 2, no. 5, pp. 204-211, 1998.

[17] S. M. J. Kelly, "Characteristic sideband instability of periodically amplified average soliton", Electronics Letters. vol. 28, no. 8, pp. 806-807, 1992

[18] A. Hasegawa, and Y. Kodama, "Guiding centre soliton", Physics Review Letters, vol. 66, no. **2**, pp. 161-164, 1991.

[19] A. Hasegawa, and Y. Kodama, "The guiding centre soliton in optical fibres", Optics Letters, vol. 15, no. 24, pp. 1443-1446, 1990.

[20] Kelly, S. M. J., Smith, K., Blow, K. J., and Dorann N. J. , "Average soliton dynamics of a high gain erbium fibre laser", Optics Letters, vol. 16, no. 17, pp. 1337-1339, 1991.

[21] F. X. Kärtner, D. Kopf, and U. Keller, "Solitary-pulse stabilization and shortening in actively mode-locked lasers" J. Optical Society of America B vol.

12, no. **3,** pp. 486-, 1995.

[22] D. J. Jones, H. A. Haus, and E. P. Ippen**, "**Subpicosecond solitons in an actively mode-locked fiber laser**",** Optics Letters, vol. 21, no. **22**, pp. 1818-, 1996.

[23] C. R. Doerr, H. A. Haus, and E. P. Ippen, "Asynchronous soliton mode locking", Optics Letters, vol. 19, no. **23**, pp. 1958-, 1994.

[24] Wei-Wei Hsiang, Chian-Yu Lin, Ming-Feng Tien, and Yinchieh Lai, Optics Letters, vol. 30, no. **18**, pp. 2493-2495, 2005.

[25] Hermann A. Haus, David J. Jones, Erich P. Ippen, and William S. Wong, "Theory of soliton stability in asynchronous modelocking", J. Lightwave Technology, vol.14, no. **4**, pp. 622-627, 1996.

[26] J. P. Gordon, H. A. Haus, "Random walk of coherently amplified solitons in optical fiber transmission", Optics Letters, vol. 11, no. **10**, pp. 651-, 1986.

[27] A. Mecozzi, J. D. Moores, H. A. Haus, and Y. Lai, "Soliton transmission control" Optics Letters, vol. 16, no. **23**, pp. 1841-, 1991.

[28] L. F. Mollenauer, J. P. Gordon, and S. G. Evangelides, Optics Letters, vol. 17, no. **22**, pp. 1575, 1992.

[29] Antonio Mecozzi, Michele Midrio, and Marco Romagnoli, "Timing jitter in soliton transmission with sliding filters," Optics Letters, vol. **21**, no. 6, pp. 402- , 1996.

[30] Wei-Wei Hsiang, Chien-Yu Lin, Ng Kam Sooi, and Yinchieh Lai, "Long-term stabilization of a 10 GHz 0.8 ps asynchronously mode-locked Er-fiber soliton laser by deviation-frequency locking", Optics Express, vol. 14, No. **5**, pp. 1822-1828, 2006.

[31] W. -W. Hsiang, C. -Y. Lin, and Y. Lai, "Stable new bound soliton pairs in a 10 GHz hybrid frequency modulation mode-locked Er-fiber laser," Optics Letters, vol. 31, no. **11**, pp. 1627-1629, 2006.

[32] H. A. Haus, and Antonio Mecozzi, "Noise of mode-locked lasers", IEEE J. Quantum Electronics, vol 29, No. **3,** pp. 983-996, 1993.

[33] Ursula Keller, "Recent developments in compact ultrafast lasers", Nature, vol. 424, pp. 831-838, 2003.

[34] G. Steinmeyer, D. H. Sutter, L. Gallmann, N. Matuschek, U. Keller, "Frontiers in Ultrashort Pulse Generation: Pushing the Limits in Linear and Nonlinear Optics", SCIENCE, vol 286, pp.1507-1512, 1999.

[35] Claude Rulliére, "Femtosecond Laser Pulses", Springer.